Energy 290 (2024) 130166

Contents lists available at ScienceDirect

Energy

journal homepage: www.elsevier.com/locate/energy

Hybridized power-hydrogen generation using various configurations of Brayton-organic flash Rankine cycles fed by a sustainable fuel: Exergy and exergoeconomic analyses with ANN prediction

Najmeh Hajialigol [a,*], Abolfazl Fattahi [b,**], Nader Karimi [c], Mostafa Jamali [a], Shervin Keighobadi [d]

[a] Department of Mechanical Engineering, Hamedan University of Technology, 65155-579, Hamedan, Iran
[b] Faculty of Mechanical Engineering, University of Kashan, Kashan, Iran
[c] School of Engineering and Materials Science, Queen Mary University of London, London, E1 4NS, United Kingdom
[d] Chemical Engineering Department, Faculty of Engineering, University of Kashan, Kashan, Iran

ARTICLE INFO

Handling Editor: Henrik Lund

Keywords:
Organic flash Rankine cycle
Brayton cycle
PEM electrolyzer
Exergoeconomics
Artificial neural network

ABSTRACT

This paper investigates different configurations of organic Rankine flash cycles combined with a Brayton cycle by performing thermodynamic, exergy, and exergoeconomic analyses. The thermal energy of the cycle is produced through burning gaseous methane generated via gasification of biomass. A systematic analysis of these configurations is conducted to enhance the exergy efficiency of the cycles. Additionally, the reutilization of the thermal energy that would otherwise be wasted in the Brayton cycle contributes to a notable enhancement in the overall thermal efficiency of the combined cycle. A range of working fluids, namely m-Xylene, o-Xylene, p-Xylene, toluene, and ethylbenzene are analyzed for the organic Rankine cycle. Predictions using an artificial neural network (radial base function) are also carried out. The results indicate that the p-Xylene increases exergy efficiency more than other working fluids. Further, the improved organic Rankine cycle mitigates exergy destruction by 10 %. Although applying double flash evaporators improves the exergy efficiency by 3 %, it increases the unit cost of power generated by more than 10 %. The application of a data-driven model to predict various configurations of combined organic Rankin cycle with a Brayton cycle fed by biomass has rarely been investigated.

1. Introduction

The global shift towards renewable and sustainable energy sources has led to using more biomass as an economic and environmentally friendly energy resource. The fuels based on waste biomass offer an applicable path to reduce toxic gas emissions and decline reliance on fossil fuels. Additionally, the utilization of thermal waste energy is currently of high importance [1–3]. Compared to the traditional cycles, the organic flash Rankine cycle (OFRC) applies a low-temperature source of heat, leading to an increment in the exergy efficiency. This has been recognized as the best cycle for power generation using thermal waste sources [3–5]. The various integrations of OFRC have attracted the attention of the researchers, by involving it with other multi-generation systems, such as power, hydrogen, and/or desalination cycles.

Ho et al. [6] proposed several designs to decrease the irreversibility associated with the flashing process using ten aromatic hydrocarbons as the working fluid. They found that by splitting the flash process into two expansion processes and applying the selected aromatics, the efficiency could improve from 5 to 20 %, while using siloxanes, the improvement was limited to 2–4 %. In another study, they compared OFC and an optimized basic Organic Rankine Cycle (ORC), a zeotropic Rankine cycle using a binary ammonia-water mixture, and a transcritical CO_2 cycle [7]. Aromatic hydrocarbons showed efficient working fluid in both ORC and OFRC by providing higher turbine output power. By replacing the throttling valve with a two-phase expander higher efficiency was achieved. The throttling valve caused considerable exergy destruction. An OFRC with and without a two-phase expander and an ORC were compared by Lee et al. [8]. R245fa, R123, and o-xylene were chosen as

* Corresponding author.
** Corresponding author.
E-mail addresses: n.hajialigol@hut.ac.ir (N. Hajialigol), afattahi@kashanu.ac.ir (A. Fattahi).

https://doi.org/10.1016/j.energy.2023.130166
Received 24 August 2023; Received in revised form 29 November 2023; Accepted 27 December 2023
Available online 30 December 2023
0360-5442/© 2023 Elsevier Ltd. All rights reserved.

Downloaded from https://iranpaper.ir
https://www.tarjomano.com ترجمه تخصصی این مقاله مورد تایید ایران پیپر

Nomenclature

A	Area, m^2
C	Cost per unit of exergy, $/GJ
$\dot{C}$	Cost rate associated with an exergy stream, $/GJ
c_p	Specific heat, J/kg K
$\dot{E}$	Exergy destruction rate, kW
e	Specific exergy, J/kg
f	Exergoeconomic factor (%)
h	Specific enthalpy, kJ/kg
J^{ref}	Pre-exponential factor, A/ m^2
J_o	Exchange current density, A/ m^2
J	Current density, A/ m^2
k	Thermal conductivity, W/m. k
L	Membrane thickness, m
$\dot{m}$	mass flow rate, kg/s
$\dot{N}$	Molar mass flow rate, mol/s
PEM	Proton exchange membrane
Pr	Prandtl number
Q	Heat transfer, J
$\dot{Q}$	Heat transfer rate, W
Re	Reynolds number
R_{PEM}	Proton exchange membrane resistance, Ω
s	Specific entropy, kJ/kg k
T	temperature, K
V_{act}	activation overpotential, V
V_0	reversible potential, V
$V_{act,a}$	anode activation overpotential, V
$V_{act,c}$	cathode activation overpotential, V
V_{ohm}	Ohmic overpotential, V
W	Work, J
$\dot{W}$	Power, W
$\dot{Z}$	Cost rate associated with investment expenditures, $/h

subscripts

ex	exergy
f	fluid
P	product
th	thermal
tot	total

Greek letters

μ	Dynamic viscosity, pa. s
η	Efficiency
λ	Heat transfer coefficient, W/ m^2, k
λ_a	Water content at the anode-membrane interface, Ω^{-1}
λ_c	Water content at the cathode-membrane interface, Ω^{-1}
$\lambda_{(c)}$	Water content at location x in the membrane, Ω^{-1}
σ_{PEM}	Proton conductivity in PEM, s/m
$\sigma_{(x)}$	Local ionic PEM conductivity, s/m
ρ	Density.kg/ m^3
ε	Exergy effieciency

the working fluids. The results indicated that the exergy destruction in the cycle including the two-phase expander was much smaller than the simple cycle, while the exergy destruction of the ORC was mainly associated with the heat exchanger. Regarding exergy efficiency, the cycle with a two-phase expander set in the first and followed by ORC and OFRC. In a similar study, Li et al. [9] concluded that using a two-phase expander efficiency was enhanced in comparison to ORC. However, the ORC shows better performance than OFRC only for working fluids with low evaporation points. Rising the evaporation temperature improved the net power generation, while OFC indicated lower power production in all operating conditions. The variation trend of the efficiency was similar to that of power generation.

Mondal and De [10] proposed an OFRC including an ejector with or without a compressor. The maximum power generated and refrigeration cycle performance depended on the flash pressure. The energy efficiency of the proposed cycles was higher than the conventional OFRC. Similar research was performed by Mondal et al. [11] who repeated the preferences of using an ejector instead of a flash tank, leading to a 9.5 % increment in both energy efficiency and power output. Increasing the flash pressure from a threshold made a dramatic subside in the irreversibility. Having a lower global warming potential, butane and isopentane were proposed as fuels. Application of the ejectors in ORFC was also the subject of the study by Chen et al. [12]. The maximum exergy efficiency was achieved by using double ejectors with one flash evaporator (38.95 %) followed by the cycle applied one ejector and two flash evaporators (37.92 %). The cycle having a single ejector with a single flash evaporator showed lower exergy efficiency than the ORC. The double ejectors-double flash evaporators cycle presented the highest energy efficiency.

Hadelu and Boyaghchi [13] investigated embedding the ejectors instead of flash evaporators in OFRC. One ejector with a high or low flash temperature evaporator in the cycle was assessed. The net power, energy, and exergy efficiencies improved by respectively 16.83 %, 13.05 %, and 10.99 %, if an ejector and a high-pressure flash evaporator were utilized. However, the double-ejector cycle improved the environmental effect by 0.95 % in comparison to the other cycles used. Three architectures of the cycle using one or two ejectors associated with one or two flashes. Using R-245fa and R600 as the working fluid, two cycles of OFRC and a transcritical CO_2 power cycle that applied the low-grade thermal waste of Sulphur flue gas were compared in another study by Mondal and De [14]. Power generation for the latter was slightly higher than the former with lower environmental impacts, while the former included higher minimum bare module costs. If lower power generation was needed, OFRC showed a better economic response. Baccioli et al. [15] presented a solution for a wide heat transfer area in the heat exchangers of OFRC, stemming from the lower mean temperature difference. They used a regenerator to increase the inlet temperature of the heat exchanger. The energy efficiency of the investigated cycle was the same as that of traditional OFRC, while the cycle cost per kW power decreased by 20 %. The working fluids by long molecular chain alkanes showed the best energy efficiency; however, they were characterized by low vapor density, resulting in large expansion devices. Mosaffa and Zareei [16] used two OFRC configurations; one included a two-phase expander and the other with separate flash evaporators. Both used an internal heat exchanger. The latter configuration provided less than 2 % rise in the output power, while the former made a 37 % increase. The optimum high flashing temperature was determined to have the highest energy and exergy efficiencies; however, the low flashing temperature imparted no change in the efficiencies.

Wu et al. [17] analyzed the exergoeconomics and provided optimization of a combined carbon dioxide Brayton cycle with an ORFC. The organic fluid absorbs waste heat from the supercritical carbon dioxide. Applying ORFC instead of ORC increased the exergy efficiency and decreased the total product of the unit cost slightly. The highest exergy efficiency and the lowest total product unit cost were achieved using n-Nonane working fluid. Using optimization, the exergy efficiency rose by about 7 % when OFRC was applied compared to utilizing ORC. Baccioli and Antonelli [18] evaluated the off-design behavior of two configurations for OFRC; the liquid out of the flash evaporator was mixed with the outlet vapor of the expander in one cycle and the liquid

Downloaded from https://iranpaper.ir
https://www.tarjomano.com ترجمه تخصصی این مقاله مورد تایید ایران پیپر

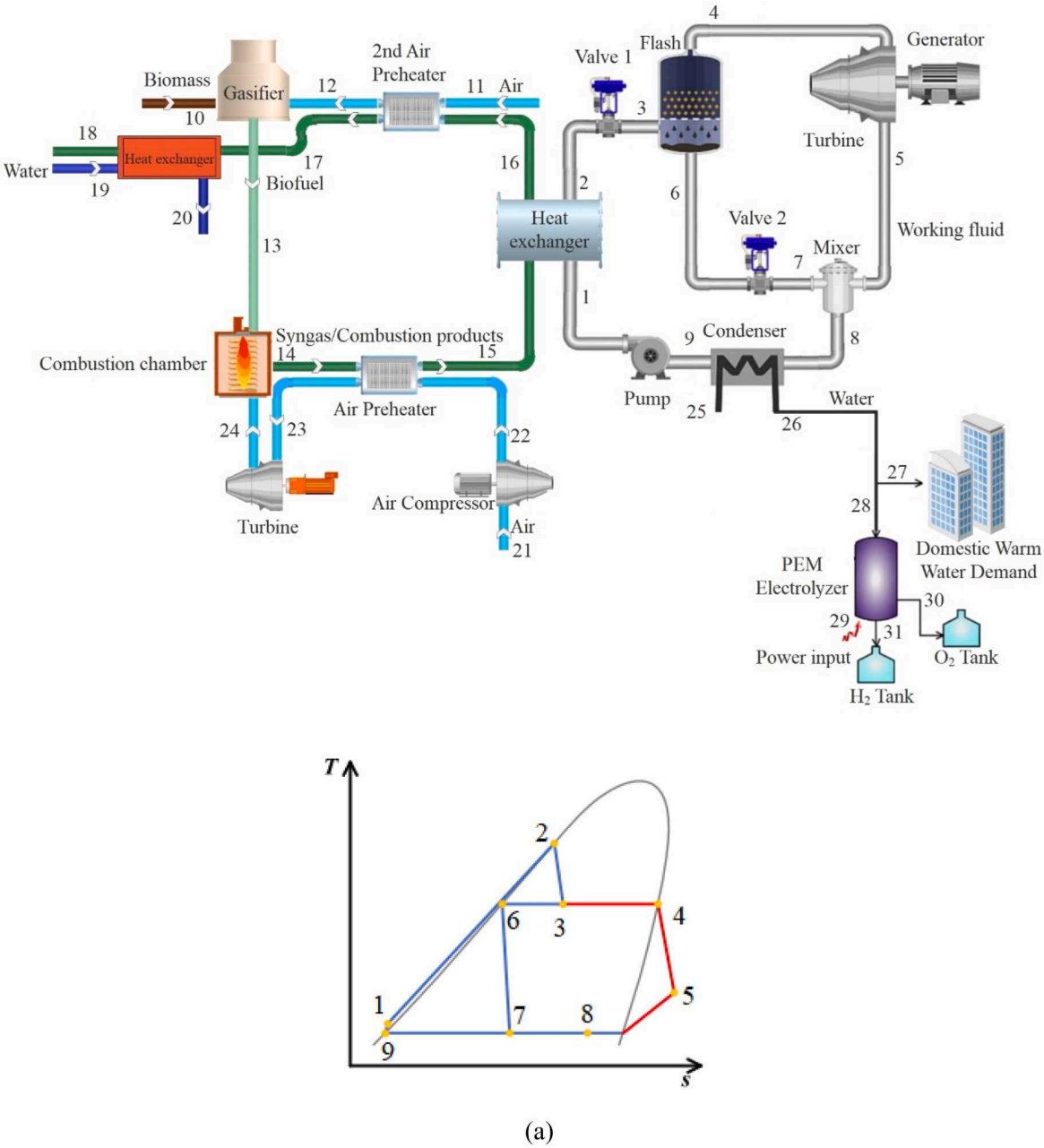

(a)

Fig. 1. The total cycle configuration and T-s diagram (Ref. [30]) of (a) SOFRC, (b) ODFRC, and (c) IOFRC.

out of the flash evaporator was mixed with the condenser liquid in the other. The i-Pentane was proposed as the efficient working fluid, stemming from lower vapor mass flow rate reduced the size of the condenser and expander. Zheng and Cao [19] examined four cycles, including an OFRC, associated with an air conditioning system to recover waste thermal energy. Through that combination, the COP was increased by 15–30 %. The ORC showed better energy efficiency compared to the other cycles applied. Making a temperature matching for two heat-transferring fluids in the heat source. Zhao et al. [20] applied the organic flash cycle, ejector refrigeration cycle, internal heat exchanger, and zeotropic mixtures in a proposed cycle. A mixture of R600a/R601 working fluids circulated in the cycle. The maximum exergy efficiency touched the value near 37 %, which was higher than that when the fluids were used separately. The fluid mixing also increased the cooling capacity. Nonetheless, the mixing reduced the exergy destruction in the condenser and evaporator.

Artificial intelligence (AI), encompassing machine learning, neural networks, and optimization algorithms, has the capacity to learn, adapt, and make informed decisions based on the patterns observed in complex data. These capabilities make AI a valuable tool for analyzing large datasets, optimizing performance, and enabling intelligent control of thermodynamic cycles.

This tool can be beneficial in enhancing the performance, control, and optimization of thermodynamic cycles [21]. By incorporating AI into control strategies, complex cycles can dynamically adapt to varying conditions, leading to enhanced operational efficiency and system robustness [21]. Therefore, it is evident why the application of AI in thermodynamic cycle design is the subject of various studies.

Liu et al. [22] proposed a combined cycle fed by a biomass-based Brayton cycle with an OFRC and a modified Kalina cycle, as well as a Claude hydrogen liquefaction unit. The output of the sensitivity analysis showed that the combustion chamber output temperature principally

Downloaded from https://iranpaper.ir
https://www.tarjomano.com ترجمه تخصصی این مقاله مورد تایید ایران پیپر

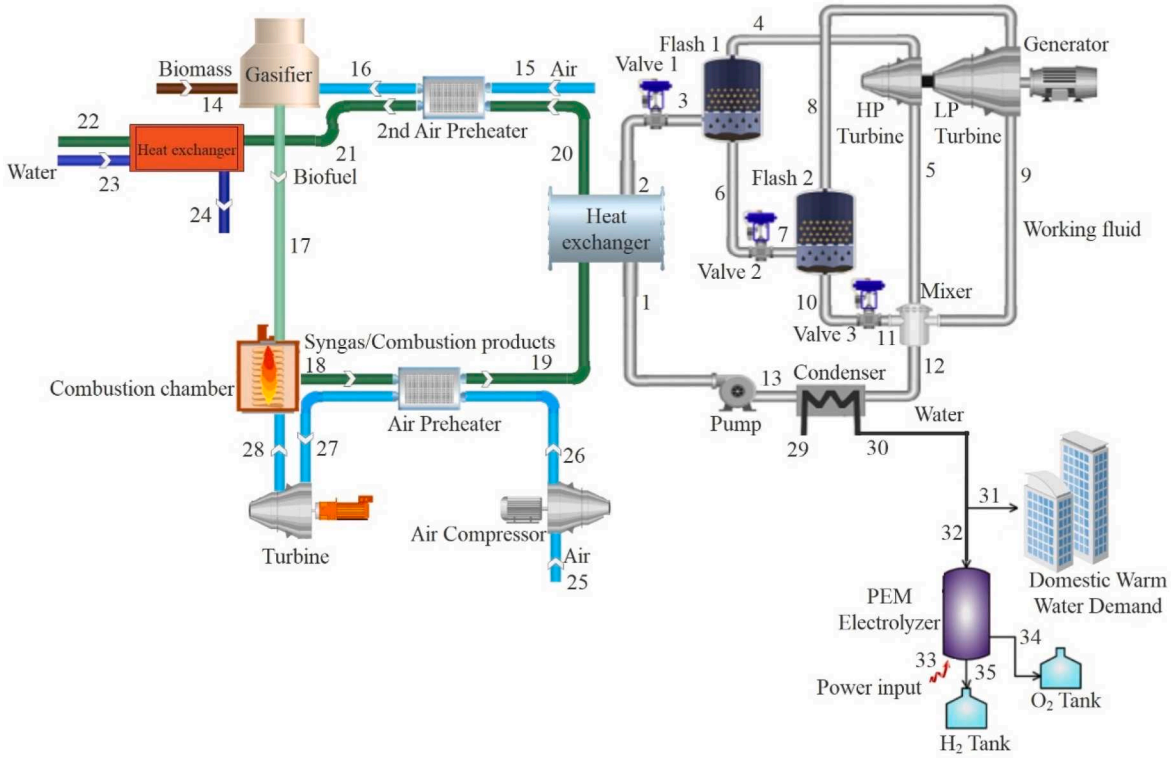

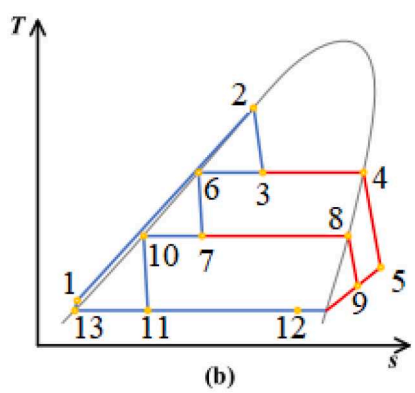

(b)

Fig. 1. (*continued*).

influenced the cycle's efficiency. The best operating conditions were determined using multi-objective optimization. A novel OFRC was 3E analyzed and optimized using the particle swarm optimization (PSO) method by Wang et al. [23]. The maximum exergy lost belonged to the condenser followed by the evaporator. More than 60 % of capital investment was specified for expanders. The working fluids with higher critical temperatures elevated the cycle with higher efficiency and lower cost. Although the OFRC highlighted a better thermodynamic performance, its thermoeconomic performance was weaker than those of ORC. Addressing the potential of novel OFRCs with or without a regenerator, the PSO algorithm was applied by Wang et al. [24]. The most significant exergy lost was found for the throttling process, while the largest thermal energy vanished from the heat recovery system. Based on a machine learning approach, one of the proposed cycles became the most efficient. Wang et al. [25] implemented a multi-objective optimization for a combination of OFRC, refrigeration, and thermal energy storage units. Increasing the evaporation temperature enhanced the energy efficiency. The condenser, turbine, and compressor were characterized by the highest cost.

A combined CCHP and OFRC was optimized using a genetic algorithm and the random forest algorithm by Ai et al. [26]. The latter reduced the optimization time drastically. The environmental and economic assessment was also performed. An OFRC was upgraded using an absorption chiller and a proton exchange membrane fuel cell (PEMFC) by Hai et al. [27]. A three-objective optimization was performed for the exergy efficiency, payback period, and net cost value. The exergy efficiency was 39.39 % and the exergoeconomic factor took the value of 60.12 %. Tang et al. [28] optimized a combined supercritical CO_2 Brayton-OFRC. The multi-objective optimization indicated that using OFRC could improve the exergy efficiency by more than 1 % compared to the basic organic flash cycle. A geothermal steam flash cycle with an absorption refrigerator was optimized using the Genetic-Fgoalattain algorithm by Zhou et al. [29]. To decrease the heat loss in the cycle, they embedded an expander and thermoelectric generators instead of

Downloaded from https://iranpaper.ir
https://www.tarjomano.com ترجمه تخصصی این مقاله مورد تایید ایران پیپر

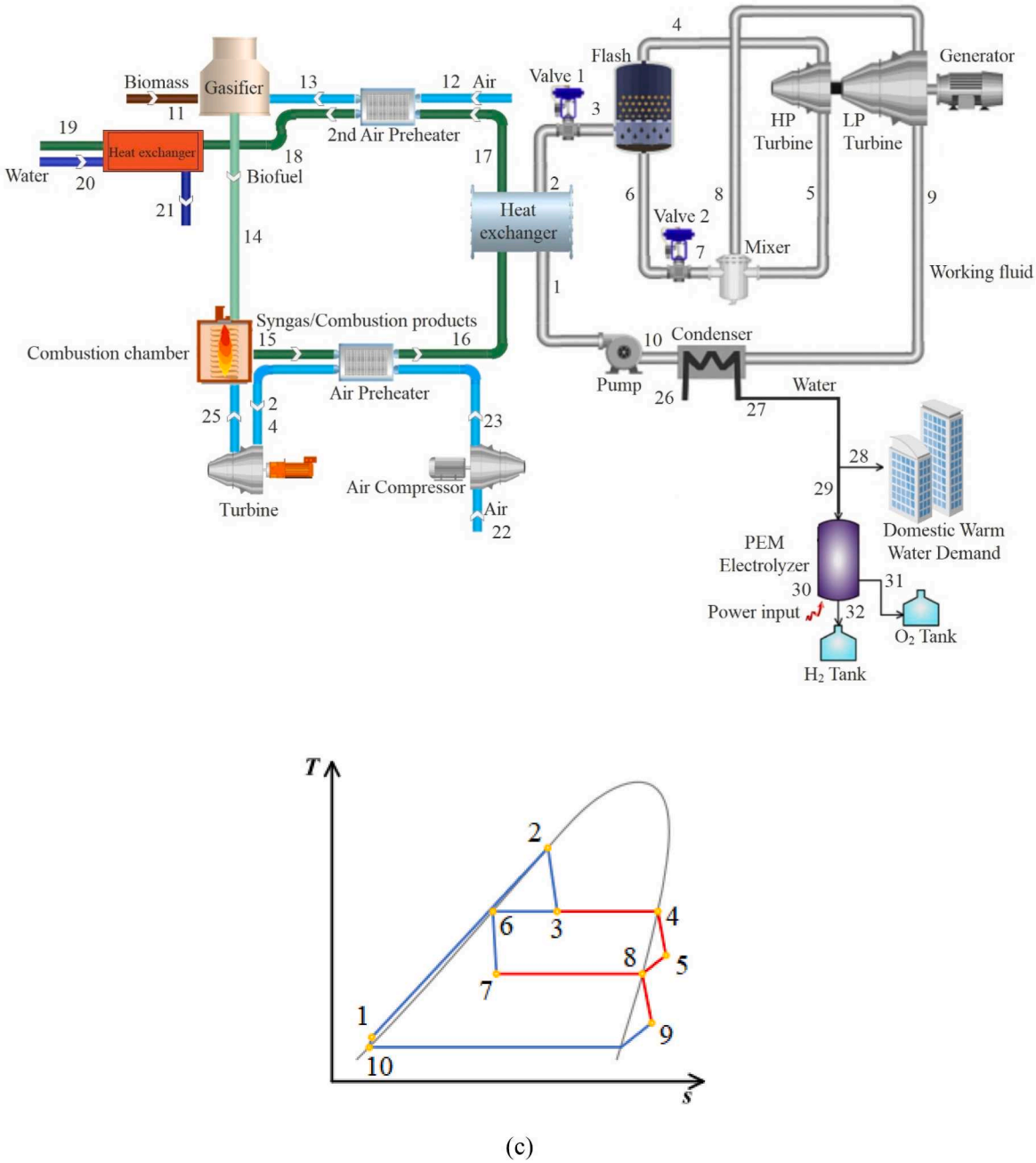

(c)

Fig. 1. (*continued*).

the throttling valve and condenser, respectively. Further, an electrolysis produced hydrogen. The optimized exergy efficiency of the system reached about 31 %, which was almost 15 % higher than the basic OFRC. The proposed system was superior to the sole OFRC from the economic view.

The integration of a biomass gasifier to produce biofuel, a Brayton cycle, an ORFC, and PEM hydrogen production presents a synergistic approach to sustainable energy conversion and waste thermal energy use in the current study. Referring to the literature review, a combination of such cycles by a data-driven predictor model has not been considered in the past. If designed properly, the proposed cycles can enable efficient utilization of biomass fuel by effectively converting thermal energy into electricity and hydrogen without emitting significant greenhouse gases. Applying biomass energy in a Brayton cycle and recovering the waste heat in an OFRC makes a novel passway to produce power from agricultural and food wastes, making the proposed cycle different from the conventional cycles. The resultant hybridized system also provides hot water for residential use. Various configurations of OFRCs are examined and by applying ANN, accurate predictions are made for the main parameters of the cycle.

2. System description and modeling

2.1. The cycles configuration

Fig. 1 introduced different configurations of OFRC applied in the current multi-generation cycle as well as the temperature-entropy diagrams of the Rankine cycles. In the top left, the gasification reactor produces the gaseous biomass-driven fuel aiding the fed air preheated earlier in the second air preheater. The extracted biofuel is burnt in the combustion chamber with air provided by the Brayton cycle. The combustion products lose the heat in four stages; two air preheaters and two

Downloaded from https://iranpaper.ir
https://www.tarjomano.com ترجمه تخصصی این مقاله مورد تایید ایران پیپر

Table 1
Thermodynamic properties of selected working fluids [31].

Working fluid	Critical temperature (K)	Critical Pressure (kPa)
Toluene	591.75	4126
O-Xylene	630.26	3738
Ethylbenzene	617.1	3622
M-Xylene	616.9	3535
P-Xylene	616.16	3532

heat exchangers. The first air preheater provides thermal energy for the working fluid of the Brayton cycle out of the combustion products. The waste thermal energy is used in the OFRC through the heat exchanger. The burned gases warm the air coming into the gasifier by the second air preheater and finally, it produces a hot water line. Power generation is provided in the OFRC and Brayton cycle, used for proton exchange membrane (PEM) and residential districts. Three configurations for OFRC are studied, as the simple OFRC (SOFRC), dual flash (ODFRC), and improved OFRC (IOFRC), presented in Fig. 1 a to c, respectively. The flash evaporator aids in separating the vapor and liquid at low temperatures. The heat transfer in the heat exchanger (from 1 to 2) is such that the liquid at the outlet becomes saturated. After decreasing the pressure by the throttling valve 1 (from 2 to 3), the vapor out of the flash is expanded in the high-pressure turbine (from 4 to 5). The pressure of the saturated liquid of the flash falls down using the throttling valve 2 and is prepared to enter the mixer and blend with the turbine outlet flow for SOFRC and IOFRC, or enter the flash 2 for ODFRC. The resultant mixer flow feeds to the condenser in the SOFRC and ODFRC or the low-pressure turbine in the IOFRC. In the ODFRC, the saturated liquid out of the first flash feeds flash 2 after breaking its pressure by the second throttling valve. Flash 2 provides the vapor for the low-pressure turbine. The inlet of the low-pressure turbine is in saturated vapor conditions, while the outlet of the high-pressure turbine should be superheated [11]. Therefore, the working fluid should be dry in the cycles to keep such conditions. The cooling fluid line of the condenser suits the water for buildings and PEM. The hydrogen and oxygen generated by the PEM electrolyzer are separately stored in the tank, as the other production of the proposed cycles to cool down to the environmental temperature.

2.2. Assumptions

For modeling the proposed cycles, the following assumptions are essential.

- Steady-state operating conditions,
- No heat loss in the heat-transferring components,
- Negligible kinetic and potential exergy in the components,
- Considering the values of 298K and 1 bar respectively for the dead state,
- Neglecting the change in the potential and kinetic energy and exergy,
- Neglecting pressure drop in the components and pipelines,
- Neglecting frictional loss in the pipes and components,
- Considering the isentropic efficiency of 85 % for pump, compressor, and turbines.

2.3. Working fluids

The selected organic working fluids should have a high critical temperature and be dry. Those fluids used in the current study and their thermodynamic properties are demonstrated in Table 1.

2.4. Gasifier analysis

By adding heat, a gasifier reuses a portion of CO_2 produced in the gasifying system to produce methane in the gaseous phase, corresponding to the following equation.

$$CH_aO_bN_c + wH_2O + \dot{n}_{CO_2}CO_2 + \text{Heat} \rightarrow \dot{n}_{H_2}H_2 + \dot{n}_{CO}CO + \dot{n}_{CO_2}CO_2O + \dot{n}_{H_2O}H_2O + \dot{n}_{CH_4}CH_4 \quad (1)$$

The $CH_aO_bN_c$ is representative of the biomass fuel and w shows the moisture associated with the organic textures. With the main reaction, simultaneous two equilibrium reactions also occur.

$$\text{Water gas shift WGS}: CO + H_2O \leftrightarrow CO_2 + H_2 \text{ - } 41166 \text{ kJ/kmol} \quad (2)$$

Methane reforming MR

$$CH_4 + H_2O \leftrightarrow CO + 3H_2 \text{ - } 205813 \text{ kJ/kmol} \quad (3)$$

More details including the equilibrium constants can be found in Refs. [32,33]. The biomass content is considered as wood, paper, and municipal solid waste. The atomic composition of the biomass content is also described in Ref. [32].

2.5. Modeling of PEM electrolyzer

The PEM electrolyzer requires heat and electricity to produce hydrogen and oxygen. In the purposive cycles the heat is provided by the condenser and the electricity is made by the generators coupled with the turbines. The hydrogen and oxygen are produced in respectively cathode and anode. The total required energy for this process is the summation of the thermal energy ($T\Delta S$) and Gibbs free energy (ΔG), presented by

$$\Delta H = \Delta G + T\Delta S \quad (4)$$

The molar hydrogen and oxygen produced are determined as follows.

$$\dot{N}_{H_2} = \frac{J}{2F} \quad (5)$$

$$\dot{N}_{O_2} = \frac{J}{4F} \quad (6)$$

in which J and F respectively stand for the electrical current and Faraday constant. By considering $J < 10,000 A/m^2$, the overpotential occurrence is negligible [34]. The PEM electrolyzer voltage encompasses the reversible potential (V_0), anode activation overpotential ($V_{act,a}$), cathode activation overpotential ($V_{act,c}$), and electrolyte ohmic overpotential (V_{ohm}), which reads

$$V = V_0 + V_{act,a} + V_{act,c} + V_{ohm} \quad (7)$$

The Nernst equation expresses the activation overpotential, as

$$V_0 = 1.229 - 8.5 \times 10^{-4}(T_{PEM} - 298) \quad (8)$$

The local ionic conductivity of PEM is also needed, which is dependent on the local water content in the membrane ($\lambda(x)$).

$$\sigma_{PEM}[\lambda(x)] = (0.5139\lambda(x) - 0.326) \times exp\left[1,268 \times \left(\frac{1}{303} - \frac{1}{T}\right)\right] \quad (9)$$

The value of $\lambda(x)$ is defined linearly by its boundary values, as

$$\lambda(x) = \frac{\lambda_a - \lambda_c}{L}x + \lambda_c \quad (10)$$

In Eq. (10), L indicates the membrane thickness, and λ_a and λ_c denote the anode and cathode water content, respectively. The ohmic resistance and overpotential are described by

$$R_{PEM} = \int_0^d \frac{dx}{\sigma_{PEM}[\lambda(x)]} \quad (11)$$

$$V_{ohm} = JR_{PEM} \quad (12)$$

Downloaded from https://iranpaper.ir
https://www.tarjomano.com ترجمه تخصصی این مقاله مورد تایید ایران پیپر

Table 2
PEM electrolyzer important values [35].

Item	Value
The inlet temperature of the electrolyzer	343
Inlet pressure of electrolyzer, (kPa)	101.3
Current density, J (A/m^2)	3000
Water content at the anode–membrane interface, $\lambda_a(\Omega^{-1})$	14
Water content at the cathode–membrane interface, $\lambda_c(\Omega^{-1})$	10
Membrane thickness, L (μm)	100
The activation energy in the anode, $E_{act,a}(kJ/mol)$	76
The activation energy in the cathode, $E_{act,a}(kJ/mol)$	18
The pre-exponential factor of the anode, $J_a^{ref}(A/m^2)$	1.7×10^5
The pre-exponential factor of the cathode, $J_a^{ref}(A/m^2)$	4.6×10^3

The activation overpotential, meaning the potential required for water decomposition is calculated by

$$V_{act} = \frac{RT}{F} sinh^{-1}\left(\frac{J}{2J_{0,i}}\right) \quad i = a, c \tag{13}$$

in which $J_{0,i}$ is the exchange current density, defined by

$$J_{o,i} = J_i^{ref} ep\left(-\frac{E_{act,i}}{RT}\right) \quad i = a, c \tag{14}$$

Hereby, $E_{act,i}$ is the activation energy of the cathode and anode. Table 2 characterizes the PEM electrolyzer input values.

In the following sections, the governing equations are presented and discussed.

2.6. Energy equation

The components of the cycles are considered as the control volume, whose mass and energy balance are given by the following equations.

$$\sum \dot{m}_{in} = \sum \dot{m}_{out}, \tag{15}$$

$$\dot{Q}_{CV} + \sum \dot{m}_{in} h_{in} = \dot{W}_{CV} + \sum \dot{m}_{out} h_{out}, \tag{16}$$

in which $\dot{Q}$, $\dot{W}$, and h indicates respectively the heat transfer rate, power, and enthalpy. Further, $\dot{m}$ means the mass flow rate and subscripts *in* and *out* denote the inlet and outlet flow, respectively.

Thermal efficiency, which is related to the first law of thermodynamics, is defined as the following for the current cycles.

$$\eta_I = \frac{\dot{W}_{tur,Brayton} + \dot{W}_{tur,Rankine} - \dot{W}_{compressor} - \dot{W}_{pump} - \dot{W}_{PEM}}{\dot{Q}_{CC}} \tag{17}$$

The subscribe *tur* means turbine and *CC* denotes the combustion chamber.

2.7. Exergy equation

Exergy means the maximum work that can be performed by a system or control volume in a reversible process finally being in the equilibrium state with the environment. Exergy analysis is essential for each thermodynamic cycle to identify and subside the exergy destruction. Exergy calculations are also needed for the exergoeconomic analysis and for making each component to operate in the best mode. The exergy of each flow encompasses two terms, which are physical and chemical, as

$$e_i = e_{ph,i} + e_{ch,i} \tag{18}$$

The physical and chemical exergy, indexed by *ph* and *ch*, for each flow, is described by

$$e_i^{ph} = h_i - h_0 - T_0(s_i - s_0), \tag{19}$$

Table 3
Definitions of fuel and product for components of different OFC configurations.

Different OFCs	Components	Fuel	Product
SOFRC			
	Heat exchanger	$\dot{E}_{15} - \dot{E}_{16}$	$\dot{E}_2 - \dot{E}_1$
	Flash & valve 1	$\dot{E}_2$	$\dot{E}_4 - \dot{E}_6$
	Turbine	$\dot{E}_4 - \dot{E}_5$	$\dot{W}_T$
	Valve 2	$\dot{E}_6$	$\dot{E}_7$
	Condenser	$\dot{E}_8 - \dot{E}_9$	$\dot{E}_{25} - \dot{E}_{26}$
	Pump	$\dot{W}_p$	$\dot{E}_1 - \dot{E}_9$
ODFRC			
	Heat exchanger	$\dot{E}_{19} - \dot{E}_{20}$	$\dot{E}_2 - \dot{E}_1$
	Flash & valve 1	$\dot{E}_2$	$\dot{E}_4 - \dot{E}_6$
	Flash & valve 2	$\dot{E}_6$	$\dot{E}_8 - \dot{E}_{10}$
	HP turbine	$\dot{E}_4 - \dot{E}_5$	$\dot{W}_{HPT}$
	LP turbine	$\dot{E}_8 - \dot{E}_9$	$\dot{W}_{LPT}$
	Valve 3	$\dot{E}_{10}$	$\dot{E}_{11}$
	Condenser	$\dot{E}_{12} - \dot{E}_{13}$	$\dot{E}_{30} - \dot{E}_{29}$
	Pump	$\dot{W}_{pump}$	$\dot{E}_1 - \dot{E}_{13}$
IOFRC			
	Heat exchanger	$\dot{E}_{16} - \dot{E}_{17}$	$\dot{E}_2 - \dot{E}_1$
	Flash & Valve 1	$\dot{E}_2$	$\dot{E}_4 - \dot{E}_6$
	HP Turbine	$\dot{E}_4 - \dot{E}_5$	$\dot{W}_{HPT}$
	LP Turbine	$\dot{E}_8 - \dot{E}_9$	$\dot{W}_{LPT}$
	Valve 2	$\dot{E}_6$	$\dot{E}_7$
	Condenser	$\dot{E}_9 - \dot{E}_{10}$	$\dot{E}_{27} - \dot{E}_{26}$
	Pump	$\dot{W}_P$	$\dot{E}_1 - \dot{E}_{10}$

$$e_{mixture}^{ch} = \sum_i x_i e_{0,i}^{ch} + \overline{R}T_0 \sum x_i \, ln \, x_i. \tag{20}$$

In Eq. (20), $e_{0,i}^{ch}$ and x_i specifies respectively the standard chemical exergy and molar fraction of i th flow. By considering both thermodynamic laws, the exergy balance equation can be derived as follows.

$$\sum_{in} \dot{E}_i = \sum_{out} \dot{E}_j + \dot{E}_D \tag{21}$$

The terms from the left to the right are respectively the net of inlet and outlet exergy rate and the destruction rate. The last term can be defined as

$$\dot{E}_{D,k} = \dot{E}_{F,k} - \dot{E}_{P,k} \tag{22}$$

whereby $\dot{E}_{F,k}$ and $\dot{E}_{P,k}$ are exergy of the fuel and products, respectively. Additionally, the exergy efficiency is given by

$$\varepsilon_k = \frac{\dot{E}_{P,k}}{\dot{E}_{F,k}} \tag{23}$$

For the PEM electrolyzer, the exergy balance is

$$E_{D,PEM} = \dot{E}_{H_2O,in} + \dot{W}_{elec} - \left(\dot{E}_{H_2O,out} + \dot{E}_{H_2,out} + \dot{E}_{O_2,out}\right) \tag{24}$$

Table 3 tabulates the exergy of fuel and products of various components of the cycle configurations.

2.8. Exergoeconomic analysis

The exergoeconomic analysis is a thermodynamic approach to finding the effective cost of components and flows. The derived data can be obtained by considering both economic and exergy analysis. It couples the cost predictions with a thermodynamic analysis. Therefore, the exergoeconomic analysis can reflect the effects of the thermodynamic configurational change on economic matters. The main thermodynamic parameter related to the cost is exergy influenced by both the first and second laws of thermodynamics. Thus, the exergoeconomic analysis is performed subsequent to thermodynamic analysis and determining the fuel and cost exergy flow. The exergoeconomic analysis requires auxil-

iranpaper Downloaded from https://iranpaper.ir
https://www.tarjomano.com ترجمه تخصصی این مقاله مورد تایید ایران پیپر

Table 4
The exergoeconomic equations for the system components.

Different OFCs	Components	Cost balance equation	Auxiliary equation
SOFRC			
	Heat exchanger	$\dot{C}_{15}+\dot{C}_1+\dot{Z}_{HA}=\dot{C}_{16}+\dot{C}_2$	$C_{15}=C_{16}$
	Flash & valve 1	$\dot{C}_2+\dot{Z}_{F\&V}=\dot{C}_4+\dot{C}_6$	$\frac{\dot{C}_4-\dot{C}_2}{\dot{E}_4-\dot{E}_2}=\frac{\dot{C}_5-\dot{C}_2}{\dot{E}_6-\dot{E}_2}$
	Turbine	$\dot{C}_4+\dot{Z}_T=\dot{C}_5+\dot{C}_W$	$C_4=C_5$
	Valve 2	–	$C_6=C_7$
	Condenser	$\dot{C}_{25}+\dot{C}_8+\dot{Z}_{cond}=\dot{C}_{26}+\dot{C}_9$	$C_8=C_9$
	Mixer	$\dot{C}_5+\dot{C}_7=\dot{C}_8$	–
	Pump	$\dot{C}_9+\dot{Z}_P+\dot{C}_w=\dot{C}_1$	$C_{w,P}=C_{w,T}$
ODFRC			
	Heat exchanger	$\dot{C}_{19}+\dot{C}_1+\dot{Z}_{HA}=\dot{C}_{20}+\dot{C}_2$	$C_{19}=C_{20}$
	Flash & valve 1	$\dot{C}_2+\dot{Z}_{(F\&V)1}=\dot{C}_4+\dot{C}_6$	$\frac{\dot{C}_4-\dot{C}_2}{\dot{E}_4-\dot{E}_2}=\frac{\dot{C}_6-\dot{C}_2}{\dot{E}_6-\dot{E}_2}$
	Flash & valve 2	$\dot{C}_6+\dot{Z}_{(F\&V)2}=\dot{C}_8+\dot{C}_{10}$	$\frac{\dot{C}_5-\dot{C}_6}{\dot{E}_5-\dot{E}_6}=\frac{\dot{C}_{10}-\dot{C}_6}{\dot{E}_{10}-\dot{E}_6}$
	HP turbine	$\dot{C}_4+\dot{Z}_{HPT}=\dot{C}_5+\dot{C}_{w,HPT}$	$C_4=C_5$
	LP turbine	$\dot{C}_8+\dot{Z}_{LPT}=\dot{C}_9+\dot{C}_{w,LPT}$	$C_8=C_9$
	Valve 3	–	$C_{10}=C_{11}$
	Condenser	$\dot{C}_{29}+\dot{C}_{12}+\dot{Z}_{cond}=\dot{C}_{30}+\dot{C}_{13}$	$C_{12}=C_{13}$
	Mixer	$\dot{C}_5+\dot{C}_9+\dot{C}_{11}=\dot{C}_{12}$	–
	Pump	$\dot{C}_{13}+\dot{Z}_P+\dot{C}_{w,P}=\dot{C}_1$	$C_{w,P}=C_{w,T}$
IOFRC			
	Heat exchanger	$\dot{C}_{16}+\dot{C}_1+\dot{Z}_{HA}=\dot{C}_{17}+\dot{C}_2$	$C_{16}=C_{17}$
	Flash & Valve 1	$\dot{C}_2+\dot{Z}_{(F\&V)1}=\dot{C}_4+\dot{C}_6$	$\frac{\dot{C}_4-\dot{C}_2}{\dot{E}_4-\dot{E}_2}=\frac{\dot{C}_5-\dot{C}_2}{\dot{E}_6-\dot{E}_2}$
	HP Turbine	$\dot{C}_4+\dot{Z}_{HPT}=\dot{C}_5+\dot{C}_{w,HPT}$	$C_4=C_5$
	LP Turbine	$\dot{C}_8+\dot{Z}_{LPT}=\dot{C}_9+\dot{C}_{w,LPT}$	$C_8=C_9$
	Valve 2	–	$C_6=C_7$
	Condenser	$\dot{C}_{26}+\dot{C}_9+\dot{Z}_{cand}=\dot{C}_{27}+\dot{C}_{10}$	$C_9=C_{10}$
	Mixer	$\dot{C}_5+\dot{C}_7=\dot{C}_8$	–
	Pump	$\dot{C}_{10}+\dot{Z}_P+\dot{C}_{w,P}=\dot{C}_1$	$C_{w,P}=C_{w,T}$

iary equations. The balance equation for cost, sought to be solved in this study, is composed of the inlet and outlet cost as well as operating and maintenance cost, which reads [36].

$$\sum_e \dot{C}_{e,k}+\dot{C}_{w,k}=\dot{C}_{q,k}+\sum_i \dot{C}_{i,k}+\dot{Z}_k \tag{25}$$

where e and i respectively indicate the inlet and outlet cost stream of component k. w and q address individually the related cost of work and heat. The cost rate is related to the exergy rate as

$$\dot{C}_j=c_j\dot{E}_j. \tag{26}$$

$\dot{Z}_k$ in Eq. (25) shows the capital cost investment rate, given by

$$\dot{Z}_k=CRF\times\frac{\Phi_r}{N\times 3600}\times Z_k. \tag{27}$$

hereby N, and Z_k and Φ_r elucidates, respectively the annual operating hours of the system, the purchased equipment cost, and the maintenance factor, set to 1.06 [37]. CRF levelized capital recovery factor, calculated by

$$CRF=\frac{i(1+i)^n}{(1+i)^n-1}, . \tag{28}$$

whereby i and n mean the interest rate and expected life cycle respectively, specified by the value of 12.4 % and 20 years [37]. As stated earlier, the coding of the cycle needs auxiliary equations to be closed, presented in Table 4 as well as the other exergoeconomic equations. In this study, the codes were written in the EES (Engineering Equations Software).

The prominent parameters in the exergoeconomic analysis are the average cost per unit product exergy ($C_{P,k}$), the average cost per unit of fuel exergy ($C_{F,k}$), the exergoeconomic factor (f_k), and the cost flow rate related to the exergy destruction ($\dot{C}_{D,k}$), which are

$$C_{P,k}=\frac{\dot{C}_{P,k}}{\dot{E}x_{P,k}} \tag{29}$$

$$C_{F,k}=\frac{\dot{C}_{F,k}}{\dot{E}x_{F,k}} \tag{30}$$

$$f_k=\frac{\dot{Z}_k}{\dot{Z}_k+\dot{C}_{D,k}} \tag{31}$$

$$\dot{C}_{D,k}=C_{F,k}\dot{E}x_{D,k} \tag{32}$$

The total exergoeconomic factor is defined by [38].

$$f_{overall}=\frac{\dot{Z}_{overall}}{\dot{Z}_{overall}+\dot{C}_{D,overall}} \tag{33}$$

where the *overall* subscript denotes the summation of all system components. Table 4 outlines the exergoeconomic equations for various OFRCs used in this study.

For the PEM electrolyzer, the cost balance and auxiliary equations are

$$\dot{C}_{H_2}+\dot{C}_{O_2}+\dot{C}_{H_2O,out}=\dot{Z}_{PEM}+\dot{C}_{power,PEM}+\dot{C}_{H_2O,in}$$

$$\dot{C}_{power,pem}=c_{power}\dot{W}_{elec}$$

$$c_{H_2O,in}=c_{H_2O,out}=0 \tag{34}$$

3. Artificial neural network

Artificial neural networks (ANN), inspired by the structure and functioning of the human brain, are powerful computational models that learn from data and make predictions or classifications. Radial basis function (RBF) is a class of ANN that excels in function approximation tasks, particularly in capturing complex relationships between input and output variables. One of the key advantages of using ANNs with RBFs in predicting thermodynamic parameters is their ability to handle nonlinear, complex, and high-dimensional datasets. Traditional thermodynamic models often rely on simplified assumptions and linear relationships, limiting their accuracy and applicability in complex systems. ANNs equipped with RBFs can capture intricate nonlinear behaviors and provide more accurate predictions, even in the absence of explicit mathematical relationships. The hidden layer works with basic radial functions and the output layer contains a sigmoid function. The RBF is formed by three layers; input, hidden, and output layer, as demonstrated in Fig. 2.

The input layer receives the data fed into the RBF without any change. In the hidden layer, the Gaussian function is applied to make the values of the layer by the following relation.

Downloaded from https://iranpaper.ir
https://www.tarjomano.com ترجمه تخصصی این مقاله مورد تایید ایران پیپر

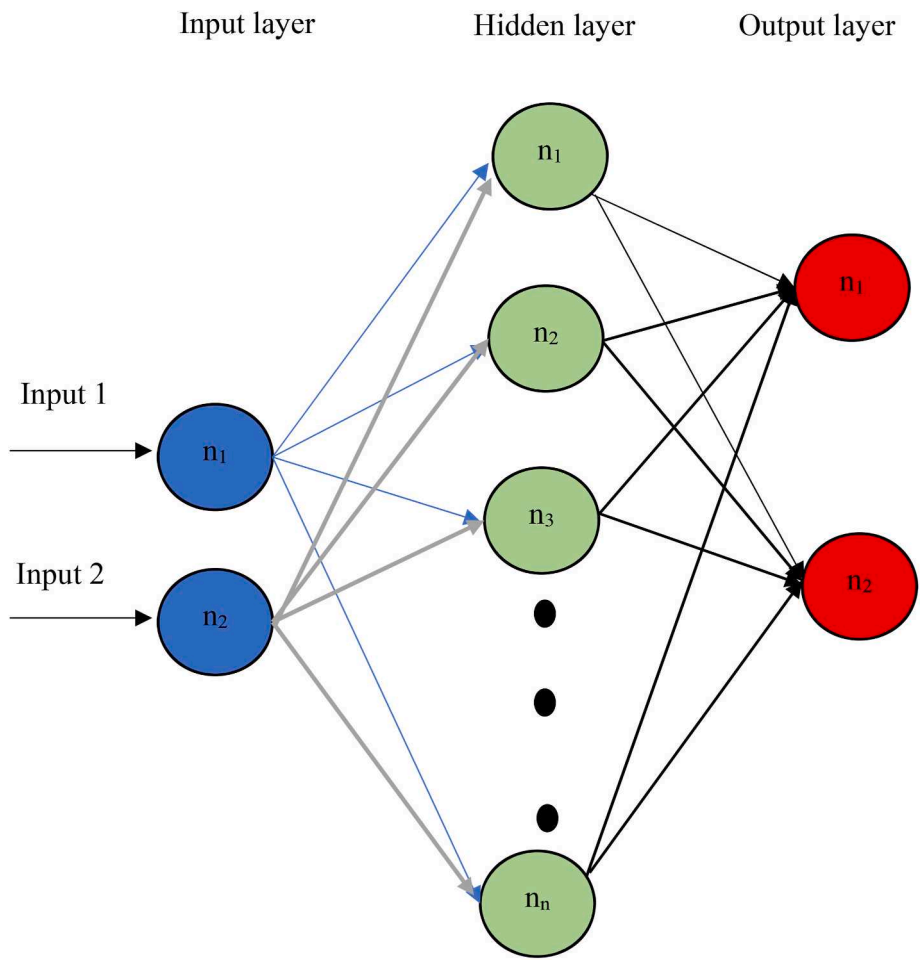

Fig. 2. The schematic connected layers of an ANN.

Table 5
A comparison of the gasification results between the current study and those released by Garcia et al. [41].

CO_2/B (g/g)	Syngas composition (%)	Data of Ref. [41]	The current results	The deviation (%)
0.94	H_2	26.96	27.03	0.25
	CO	43.48	43.87	0.89
	CO_2	27.05	26.45	2.22
	CH_4	1.75	1.86	6.28
1.09	H_2	30.66	30.21	1.47
	CO	48.79	48.95	0.32
	CO_2	19.40	19.12	1.44
	CH_4	0.86	0.91	5.81
1.13	H_2	31.22	30.98	0.77
	CO	49.97	50.06	0.18
	CO_2	17.98	17.59	2.17
	CH_4	0.97	1.12	15.46
1.34	H_2	24.96	25.08	0.48
	CO	46.14	46.23	0.19
	CO_2	27.80	28.14	1.22
	CH_4	0.76	0.80	5.26

$$h_i = \varphi_i(X - \mu_i) = \exp\left(-\frac{\|X - \mu_i\|}{2\sigma_i^2}\right), \tag{35}$$

where the X indicates the input array, μ_i and σ_i respectively specifies the center of region and width of the receptive field of the neuron, indexed by i. The output layer receives a linear combination of the weights and hidden layer values, as

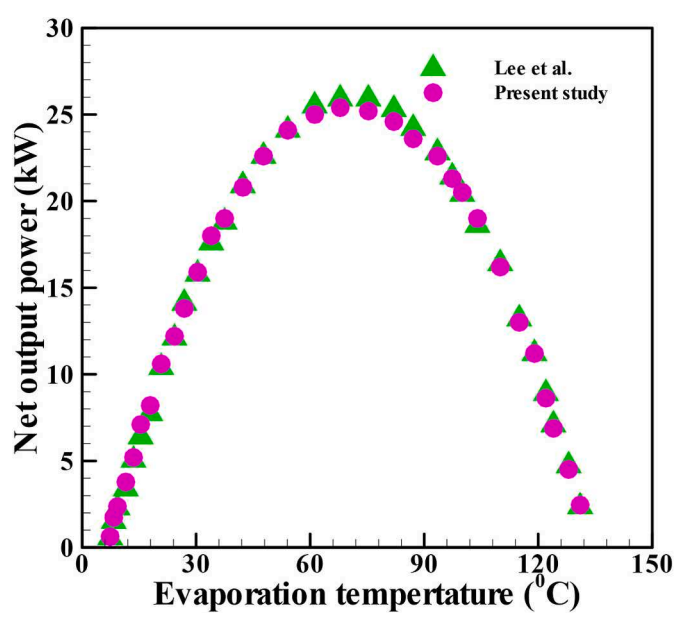

Fig. 3. A comparison between the current results and those published by Ref. [8]: the net output power versus the evaporation temperature.

Downloaded from https://iranpaper.ir
https://www.tarjomano.com ترجمه تخصصی این مقاله مورد تایید ایران پیپر

Table 6
A comparison between the current results and those published by Ref. [31]: the cell potential voltage versus the PEM electrolyzer current density.

PEM electrolyzer current density, J (A/m^2)	Cell potential voltage (V) [31]	Cell potential voltage (V) of the current work	The deviation (%)
165.137	1.698	1.681	1.00
366.972	1.754	1.801	2.68
568.807	1.792	1.769	1.28
788.991	1.802	1.782	1.11
990.826	1.821	1.802	1.04
1486.238	1.868	1.851	0.91
1981.651	1.887	1.862	1.32
2990.826	1.945	1.939	0.31
4000	1.965	1.964	0.05
4990.826	2.004	2.011	0.35

$$s = \sum_{i=1}^{k} w_i h_i(X). \tag{36}$$

The sigmoid, as an activation function, then affects the summation and makes the output. Two learning methods are required for RBF; the first for μ_i and σ_i and the second for the weights. The self-organized algorithm [39] is used for the first and the error backpropagation algorithm [39,40] is utilized for the second.

4. Code verification

The gasifier operation is first evaluated in the verification section. Table 5 releases a comparison of the syngas composition calculated in the current code with those earlier published by Garcia et al. [41]. The comparison is conducted for various ratios of carbon dioxide to biomass. The assumption of equilibrium makes a disparity, as the results are compared to the experimental data of Ref. [41]. The deviation presented

Table 7
Exergy destruction and exergy efficiency of SOFRC components for different working fluids.

	Toluene		o-Xylene		Ethylbenzene		m-Xylene		p-Xylene	
	$T_{3.opt=}$468.3 K		$T_{3.opt=}$462.8 K		$T_{3.opt=}$460.1 K		$T_{3.opt=}$461.8 K		$T_{3.opt=}$461.9 K	
	$P_{3.opt=}$550.2 kPa		$P_{3.opt=}$236.1 kPa		$P_{3.opt=}$296.3 kPa		$P_{3.opt=}$289.5 kPa		$P_{3.opt=}$292.6 kPa	
	$\dot{E}_D$ (kW)	ε (%)	$\dot{E}_D$ (kW)	ε (%)	$\dot{E}_D$ (kW)	ε (%)	$\dot{E}_D$ (kW)	ε (%)	$\dot{E}_D$ (kW)	ε (%)
Heat exchanger	89.52	69.21	95.38	66.7	90.5	67.1	91.35	68.1	88.31	68.9
Flash & Valve	21.25	40.1	23.47	39.52	22.14	40.01	22.11	41.02	21.05	40.03
Turbine	19.87	87.2	23.4	87.91	21.11	87.51	19.98	86.9	19.21	87.06
Valve 2	7.58	19.87	8.25	19.60	7.89	19.71	8.1	19.72	7.14	19.78
Condenser	20.84	16.25	20.11	16.01	20.38	16.11	21.1	20.98	19.85	16.24
Pump	0.66	91.5	0.549	91.61	0.61	91.59	0.71	91.01	0.62	90.1
Overall	159.72	43.25	171.129	40.65	162.63	41.84	163.35	42.9	156.18	43.39

Table 8
Exergy destruction and exergy efficiency of ODFRC components for different working fluids.

	Toluene		o-Xylene		Ethylbenzene		m-Xylene		p-Xylene	
	$T_{3.opt=}$501.3 K		$T_{3.opt=}$486.3 K		$T_{3.opt=}$487.2 K		$T_{3.opt=}$498.2 K		$T_{3.opt=}$503.2 K	
	$P_{3.opt=}$1109 kPa		$P_{3.opt=}$491.2 kPa		$P_{3.opt=}$519.5 kPa		$P_{3.opt=}$526.8 kPa		$P_{3.opt=}$535.5 kPa	
	$\dot{E}_D$ (kW)	ε (%)	$\dot{E}_D$ (kW)	ε (%)	$\dot{E}_D$ (kW)	ε (%)	$\dot{E}_D$ (kW)	ε (%)	$\dot{E}_D$ (kW)	ε (%)
Heat exchanger	88.3	70.1	91.25	68.01	90.12	68.15	89.9	69.71	87.2	73.6
Flash & Valve 1	8.87	42.2	10.03	40.06	9.75	41.47	9.28	40.21	8.81	43.18
Flash & Valve 2	9.21	42.4	12.28	39.94	11.73	41.02	10.21	49.98	8.89	44.5
HP Turbine	15.82	90.9	18.32	88.11	17.21	88.73	16.32	88.13	15.32	89.74
LP Turbine	3.89	90.1	4.61	88.07	4.27	88.47	3.92	88.11	3.78	89.58
Valve 2	3.57	23.5	4.08	21.41	3.99	21.58	3.91	22.32	3.48	24.3
Condenser	23.5	17.61	27.1	16.79	26.32	16.84	24.8	16.89	22.7	18.79
Pump	0.65	90.8	0.672	90.0	0.67	90.6	0.66	89.3	0.61	90.9
Overall	153.81	45.9	168.34	42.81	164.06	43.28	159	44.87	147.31	46.28

Table 9
Exergy destruction and exergy efficiency of IOFRC components for different working fluids.

	Toluene		o-Xylene		Ethylbenzene		m-Xylene		p-Xylene	
	$T_{3.opt=}$502.5 K		$T_{3.opt=}$490.1 K		$T_{3.opt=}$498.4 K		$T_{3.opt=}$501.4 K		$T_{3.opt=}$505.1 K	
	$P_{3.opt=}$1211 kPa		$P_{3.opt=}$500.2 kPa		$P_{3.opt=}$535.6 kPa		$P_{3.opt=}$550.1 kPa		$P_{3.opt=}$552.7 kPa	
	$\dot{E}_D$ (kW)	ε (%)	$\dot{E}_D$ (kW)	ε (%)	$\dot{E}_D$ (kW)	ε (%)	$\dot{E}_D$ (kW)	ε (%)	$\dot{E}_D$ (kW)	ε (%)
Heat exchanger	87.92	72.21	90.48	68.25	89.47	69.21	88.72	70.47	86.24	74.98
Flash & Valve 1	10.49	43.1	11.98	49.21	11.08	48.11	10.78	49.51	10.02	42.23
HP Turbine	15.57	92.06	17.58	88.93	16.50	89.21	16.08	89.28	15.14	92.31
LP Turbine	3.78	90.95	4.08	88.91	3.74	89.02	3.41	89.24	3.20	92.06
Valve 2	4.49	22.42	5.03	21.95	4.95	21.48	4.87	22.01	4.11	23.25
Condenser	23.2	17.82	27.94	16.81	25.17	16.95	23.75	17.07	22.41	19.11
Pump	0.78	93.32	0.82	92.45	0.81	93.17	0.79	93.79	0.77	93.41
Overall	146.23	48.22	157.91	45.97	151.72	46.85	148.4	47.21	141.89	48.83

Downloaded from https://iranpaper.ir
https://www.tarjomano.com ترجمه تخصصی این مقاله مورد تایید ایران پیپر

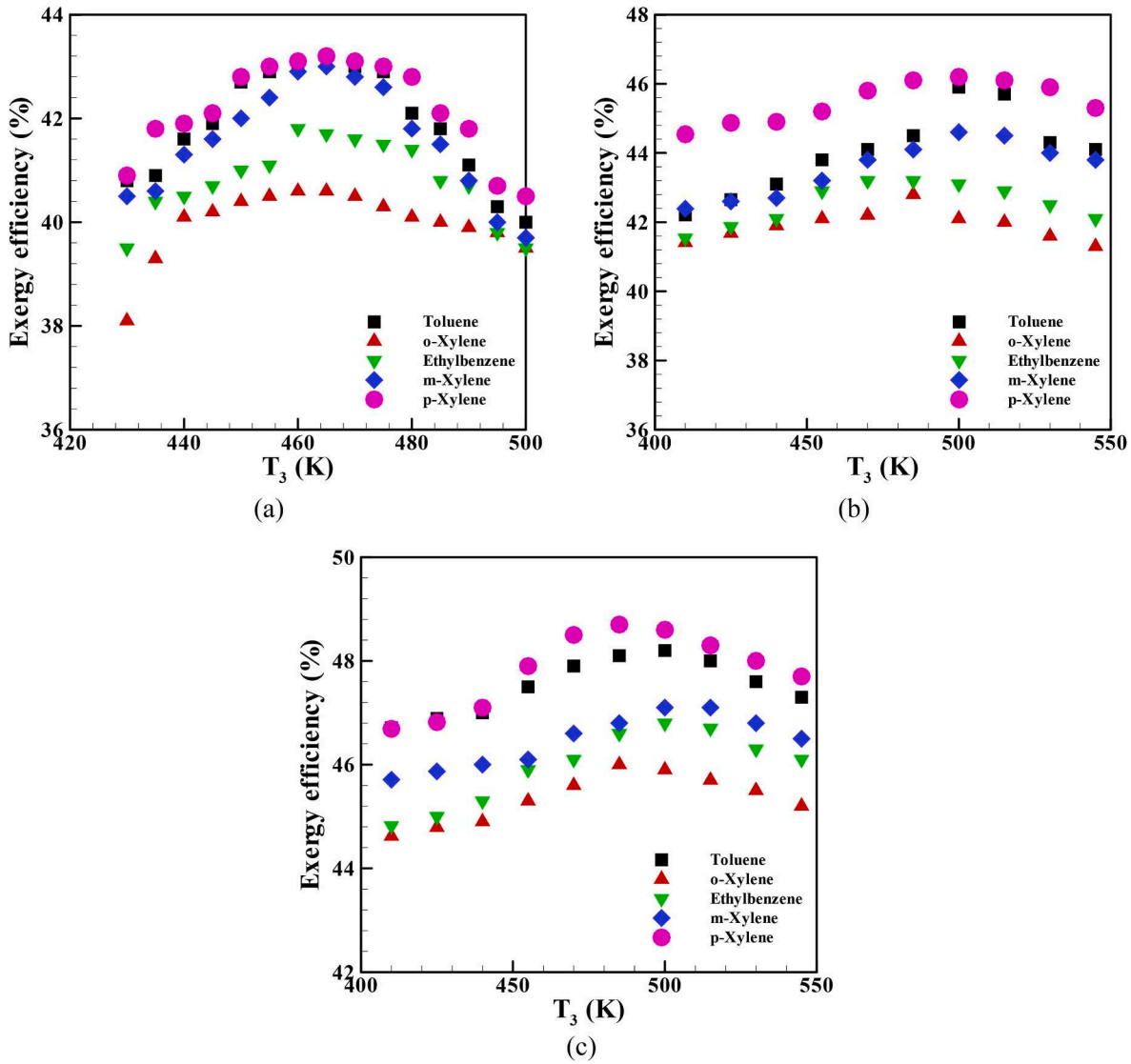

Fig. 4. The exergy efficiency versus flashing temperature for (a) SOFRC, (b) ODFRC, and (c) IOFRC.

in the last column, with an average of 2.4, 2.2, 4.6, and 1.8 %, respectively for CO_2/B of 0.94, 1.09, 1.13, and 1.34. It confirms that the code can predict the by-products of biomass gasification in the presence of the CO_2 agent.

A further comparison between the data derived from a SOFRC of Ref. [8] and the current results versus evaporation temperature is demonstrated in Fig. 3. The deviation between the two sets of data is too small and this can show that the developed computational code can truly capture the features of the OFRCs. Additionally, Table 6 elucidates a comparison for the PEM electrolyzer; the cell potential voltage concerning the electrical current density. The deviation percentage shows a good agreement with an average of 1 %.

5. Results and discussion

The exergy destruction and exergy efficiency of the configurations of the OFRC applied in the current study are presented in Tables 7–9. "Various working fluids are examined in the current study. This includes o-xylene, m-xylene, p-xylene, Toluene, and Ethylbenzene. The reasons for choosing such fluids are the appropriateness and their boiling points for ORCs, thermal stability at the operating conditions of ORCs, low Environmental Impact, and compatibility with the materials of the cycle elements."

The *opt* subscription specifies those parameters that cause the highest exergy efficiency, as discussed later. In all investigated cycles, the heat exchanger imposes the highest value of exergy destruction, ranging from about 70 to 91 kW. This stems from the large temperature difference between two heat-transferring fluids. The highest value of exergy destruction, associated with the heat exchanger, occurs when m-Xylene and o-Xylene are respectively used for the SOFRC and ODFRC. The pump is the least exergy-destructive component, with a value of less than 1 kW for all cycles. The flash and valve for SOFRC, and condenser for both ODFRC and IOFRC are the second in exergy destruction.

The exergy destruction is minimal when p-Xylene is used for all components, resulting in the lowest overall exergy destruction for all cycles. It shows that the application of a fluid with a lower evaporation temperature leads to lower exergy destruction. It is due to higher temperature gradients of the fluids with a higher saturation temperature, as before evaporation, the sensible temperature changes are considerable. The o-Xylene fluid produces the highest overall exergy destruction. The decrement in the exergy destruction by using p-Xylene compared to the case applied o-Xylene is respectively 9 %, 12.5 %, and 10 % for SOFRC, ODFRC, and IOFRC. In terms of higher exergy destruction, the investigated cycles are classified as SOFRC, ODFRC, and IOFRC. The IOFRC decreases the exergy destruction by about 10 %, compared to SOFRC. Applying a double flash prevents large temperature gradients as it

Downloaded from https://iranpaper.ir
https://www.tarjomano.com ترجمه تخصصی این مقاله مورد تایید ایران پیپر

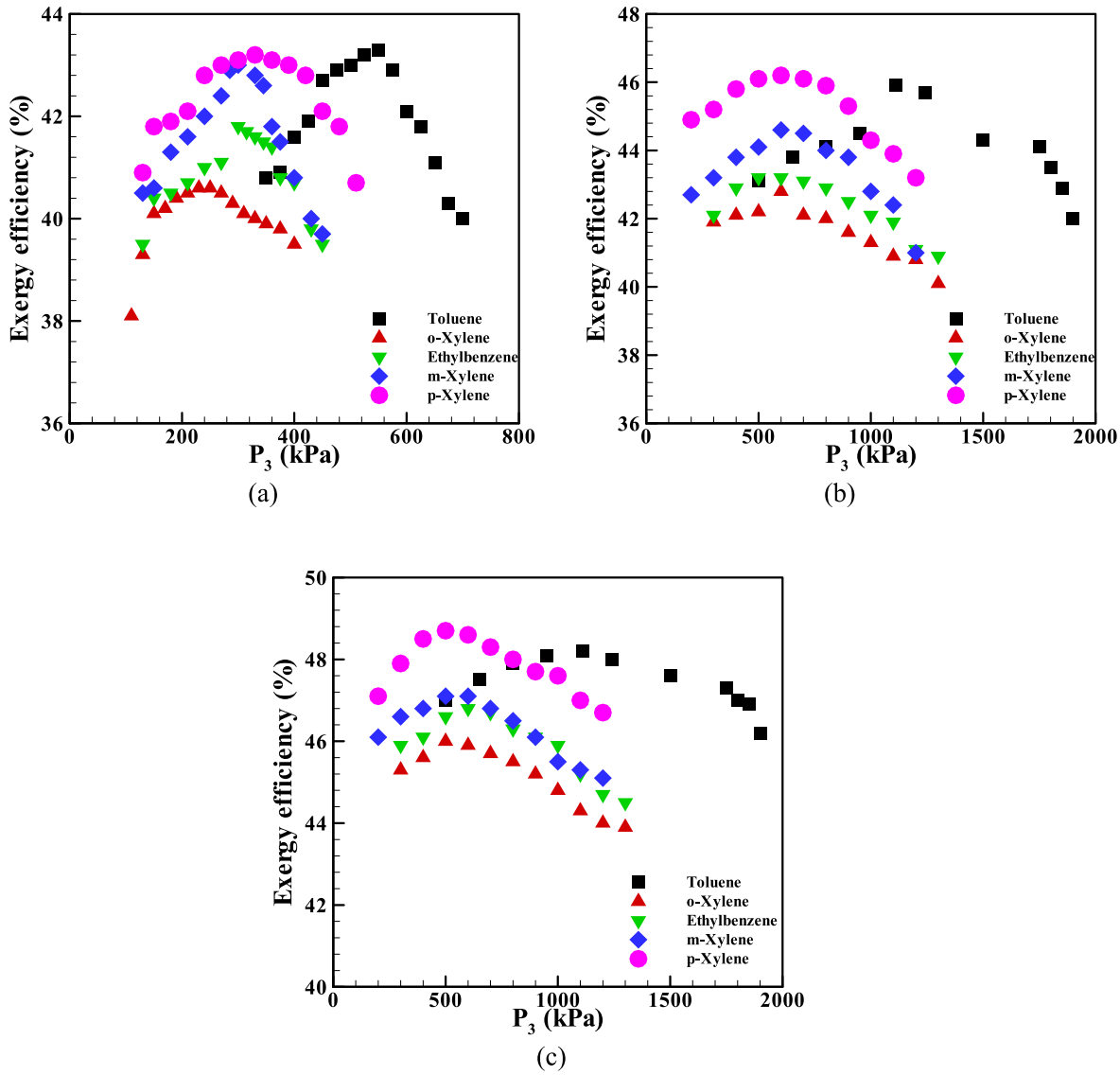

Fig. 5. The exergy efficiency versus flashing pressure for (a) SOFRC, (b) ODFRC, and (c) IOFRC.

divides the flashing process into two, leading to lower exergy destruction compared to SOFRC. Further, decreasing the valves leads to exergy destruction in the IOFRC. The maximum exergy destruction occurs in the SOFRC when o-Xylene is applied by the value of 171.129 kW, while the minimum value of 141.89 kW belongs to IOFRC with p-Xylene. Tables 7–9 also outline the exergy efficiency. As expected, the condenser and valve(s) take the lowest rank, owing to their higher irreversibility. However, the pump is ranked first. The cycles including ODFRC and IOFRC show better overall exergy efficiency compared to that of SOFRC, by a value of about 2–3 %.

The exergy efficiency for the three proposed cycles in the current study with respect to the temperature at point 3, or flashing temperature, is provided in Fig. 4. All graphs show a single-maximum trend. As expected from the data of Tables 7–9, the p-Xylene takes the highest, and o-Xylene features the lowest exergy efficiency values. Further, the exergy efficiency of the SORFC is lower than that of the other cycles, while IOFRC pretends the best exergy efficiency. It stems from the higher gradients of the thermal and pressure in the elements of SOFRC compared to the other cycles. The temperature associated with the maximum exergy efficiency is almost the same for all working fluids, except for o-Xylene and Ethylbenzene. The difference between the values of the fluids showing better exergy efficiency; Toluene, and p-Xylene show the highest values in SOFRC. Additionally, the variation trend becomes smoother in the SOFRC, which indicates lower changes in the exergy destruction of the cycle's elements to the flashing temperature. The difference between the highest and lowest values of the exergy efficiency is around 4 % on average for all investigated cycles; however, this value is lower for IOFRC. Increasing the flashing temperature intensifies the exergy of the product and it leads to an increase in exergy efficiency. However, this results in dropping the quality of the vapor and magnifies the exergy destruction [16]. Therefore, the trend seen in Fig. 4 is formed by a competition between the two effects, as explained, and it is why a single maximum trend is observed.

A similar trend of variation in Fig. 4 is found for exergy efficiency versus flashing pressure, demonstrated in Fig. 5. Similar to those presented in Fig. 4, the results of SOFRC differ from the other two cycles. A lower exergy efficiency in SOFRC is owing to higher exergy destruction; one feed line of the turbine and only one stage for expansion of the fluid flow increases the losses associated with temperature gradients and fluid irreversibility. Although there is an optimum pressure that maximizes the exergy efficiency, such optimal value varies among the working fluids. The difference among the fluids in exergy efficiency results from the variations in thermophysical properties of them making larger gradients in thermal and frictional values. The effect of applying various

Downloaded from https://iranpaper.ir
https://www.tarjomano.com ترجمه تخصصی این مقاله مورد تایید ایران پیپر

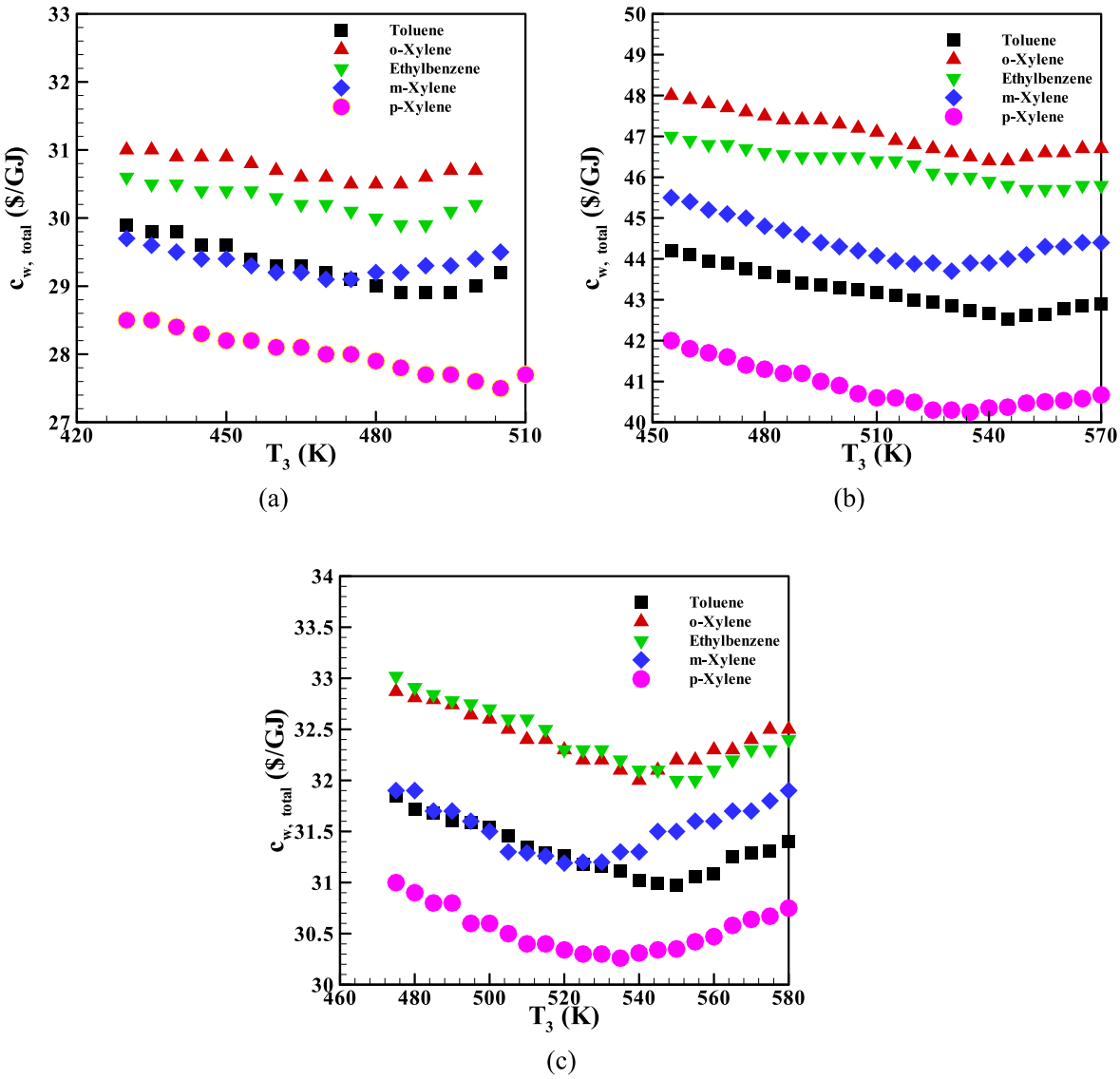

Fig. 6. Unit cost of produced power versus flashing temperature for (a) SOFRC, (b) ODFRC, and (c) IOFRC.

working fluids is less obvious in SOFRC than in the other cycles. It shows that the higher irreversibility suppresses the benefits of the fluids. Toluene, which takes the lowest evaporating temperature, shows the smoothest variation in the exergy efficiency of the ODFRC and ICFRC. The p-Xylene and toluene push the system to the nearest condition to the reversible processes if the flashing pressure is considered as the independent parameter. It indicates that the lower saturation temperature makes lower temperature gradients, leading to a higher exergy efficiency.

The unit cost of total produced power versus flashing temperature and pressure is presented in Figs. 6 and 7, respectively. The unit cost of power for the ODFRC is higher than the other two cycles by a factor of about 1.5. The p-Xylene shows the lowest unit cost to produce power followed by toluene, while o-Xylene indicates the highest. The difference in the unit power cost implies the system ranges from 6 % to 9 %, if the stated fluids are compared. The unit cost of different working fluids follows nearly the inverse trend found in the exergy efficiency. The optimum flashing temperature and pressure to have the lowest cost are different for different working fluids; toluene indicates higher values in most cases. Although it has lower exergy efficiency, the unit power cost is the lowest for SOFRC followed by IOFRC. Ethylbenzene and o-Xylene show the same variation in IOFRC. The applied fluids lead to spending less money at higher temperatures, which may be related to their high critical temperature and pressure. IOFRC and SOFRC are characterized in terms of making the minimum unit cost of m-Xylene and p-Xylene at the lowest flashing temperature and pressure. Despite the high unit power cost for ODFRC, the variation of different fluids' cost versus flashing pressure and temperature is the smoothest.

Fig. 8a illustrates the capital cost investment for the cycles investigated and working fluids in the optimum temperature, in which the unit cost of produced power is minimal. The ODFRC encounters the highest investment cost, as it involves more flash evaporators and expansion valves. $\dot{Z}_{overall}$ for ODFRC is about 50 % higher than the other cycles, on average. The IOFRC is least affected by the investment costs followed by the SOFRC. The o-Xylene imposes the highest investment cost on the cycles, contrary to the p-Xylene. By selecting the latter instead of the former, the investment cost can be mitigated by nearly 22 %, on average for all cycles. The exergoeconomic factor, defined as a measure to evaluate the effect of hidden costs compared to the investment cost, is shown in Fig. 8b. Comparing the cost of investment and exergy destruction involved in the exergoeconomic factor (see Eq. (31)), the figure indicates that higher investment cost related to the cost of exergy destruction. However, the cycles with a higher share of investment cost rank as ODFRC, SOFRC, and IOFRC. The m-Xylene working fluid in the

Downloaded from https://iranpaper.ir
https://www.tarjomano.com ترجمه تخصصی این مقاله مورد تایید ایران پیپر

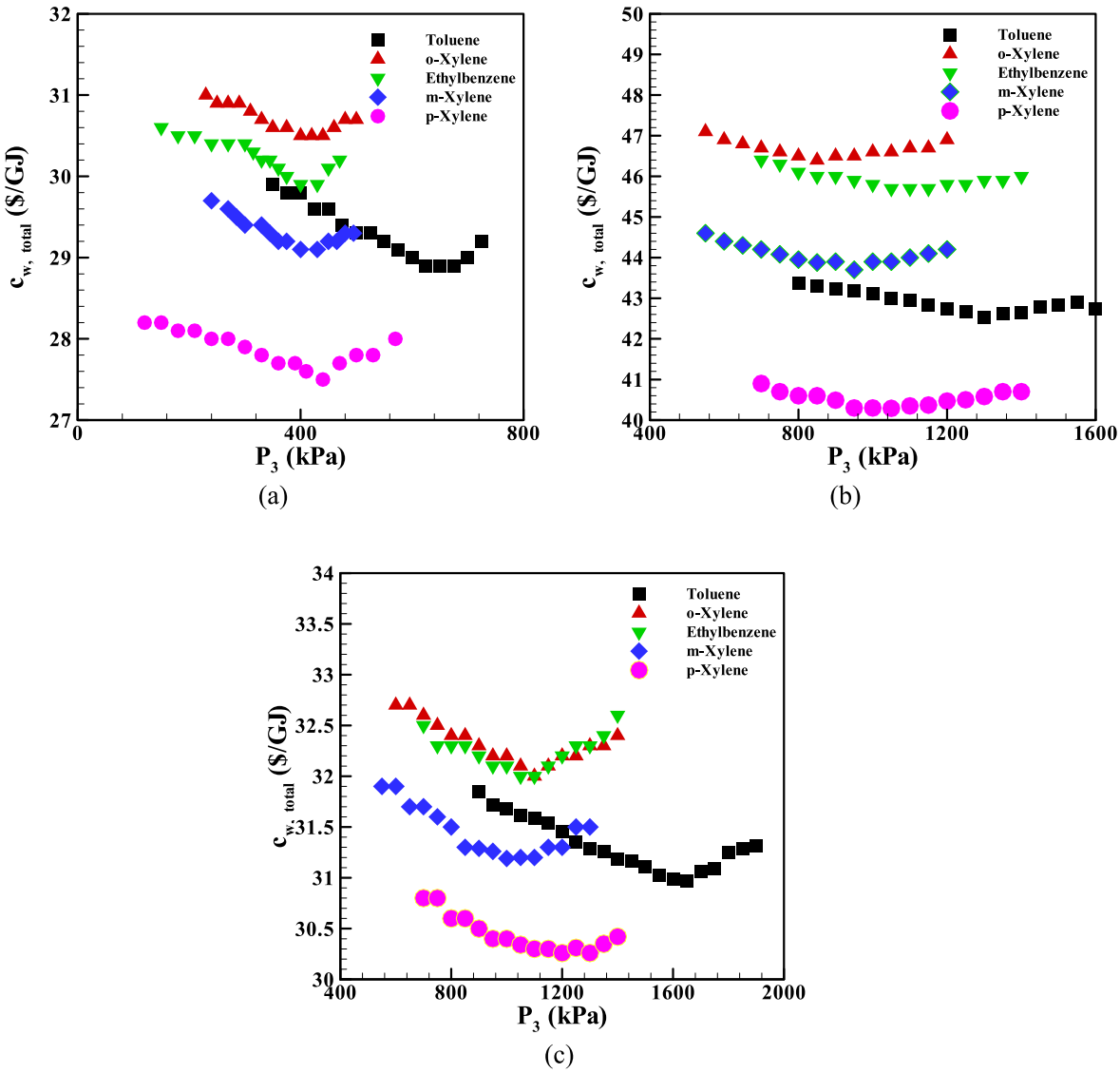

Fig. 7. Unit cost of produced power versus flashing pressure for (a) SOFRC, (b) ODFRC, and (c) IOFRC.

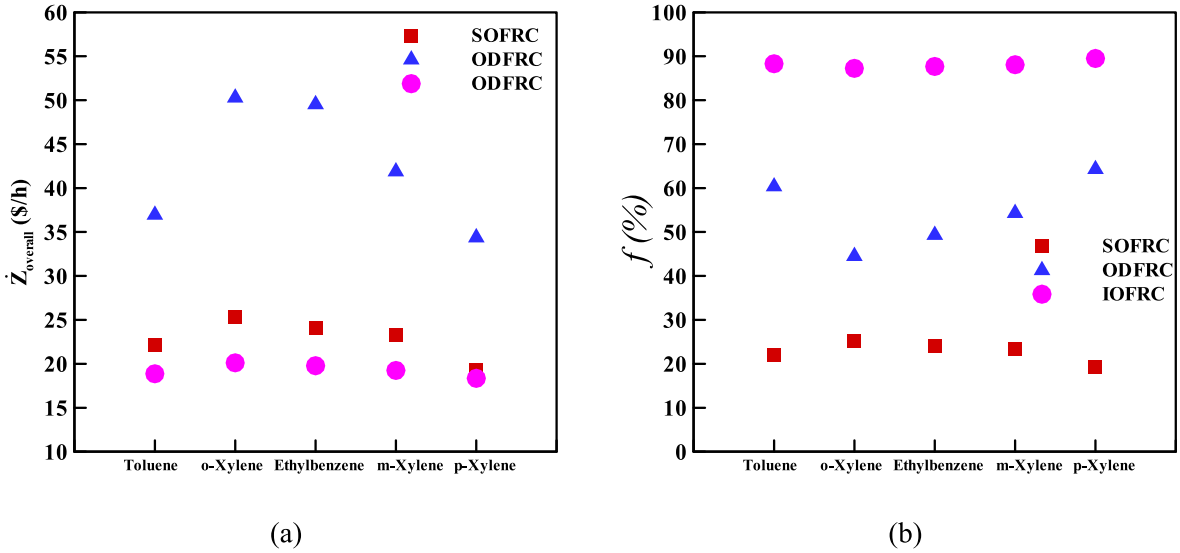

Fig. 8. Exergoeconomic parameters for different cycles and different working fluids under optimum flashing temperature (a) Capital cost investment (b) Exergoeconomic factor.

Downloaded from https://iranpaper.ir
https://www.tarjomano.com ترجمه تخصصی این مقاله مورد تایید ایران پیپر

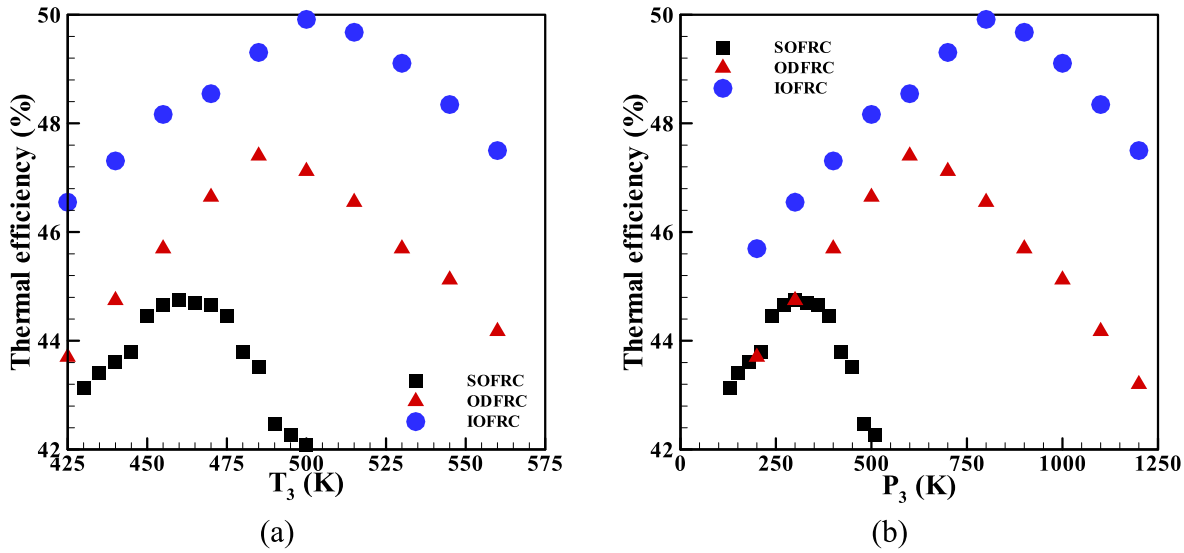

Fig. 9. Thermal efficiency of p- Xylene for different cycles studied versus (a) flashing temperature, and (b) flashing pressure.

ODFRC features almost the same share between the two costs stated earlier. The p-Xylene highlights the highest value of exergoeconomic factor.

Stemming from the best performance in exergy and exergoeconomic analysis, the thermal efficiency versus flashing temperature and pressure is presented for p-Xylene in Fig. 9. As expected, the cycles are ranked as IOFRC, ODFRC, and SOFRC in terms of having higher thermal efficiency. It is resulted from the highest power generated in the IOFRC. The flashing temperature and pressure corresponding to the highest thermal efficiency decrease following the ranking of the cycles stated above. The best flashing temperature and pressure for thermal efficiency are not the same as those for exergy efficiency. It addresses that the flashing conditions resulting in the highest power differ from those making the lowest exergy destruction. Increasing T_3 and P_3 can intensify the thermal content of the operating fluid, leading to higher power generation, by intensifying the energy content of the turbine. However, it decreases the turbine mass flow rate, which adversely affects the thermal efficiency. Choosing the most suitable flashing temperature and pressure, the thermal efficiency of IOFRC can be 4 %–6 % more than SOFRC if p-Xylene is used.

Considering the best performance, IOFRC and p-Xylene working fluid are chosen for capturing the data of the following figures. Further, the optimum values of the flashing temperature and pressure are selected, meaning those with the highest thermal or exergy efficiency. The pressure ratio influences the net power generated, as demonstrated in Fig. 10a. The compressor ratio increment from 2 to 6 aids the gas turbine power generation and higher combustion temperature. Hence, the net power and thermal efficiency pointed out in Fig. 10b, increases. The increments are around 80 % and 10 %, respectively for the former and latter. Nonetheless, the increment is smeared as the pressure ratio increases. This is owing to the higher power consumption by the compressor. Additionally, hydrogen production improves by a factor of 5, due to the effect of condenser temperature.

The effects of current density on the performance of the PEM electrolyzer is presented in Fig. 11. By increasing J from 1000 to 7000A/m^2, the net power generated subsides by about 23 % in a linear trend. The thermal efficiency also decreases by nearly 10 %. This is owing to the higher consumption of energy by the PEM electrolyzer, resulting in a decrement in the net power and thermal efficiency. Exergy efficiency also diminishes by over 10 % by raising the irreversibility in the electrochemical reaction of PEM. However, the hydrogen production increases by about 7 times as more energy is provided for water splitting.

The RBF model in the current work predicts the results. For this purpose, 10 neurons were applied in the hidden layer. The input parameters include flashing temperature and pressure. The outputs are defined as exergy efficiency and unit cost of power. 110 samples of the proposed cycles with p-Xylene working fluid were fed to the ANN for training, testing, and validation. The neuron number was evaluated to have a minimum mean absolute error (MAE). Table 10 shows the ANN prediction values versus those derived by the code for three cycles. The disparity, which is 2 and 1.43 % on average respectively for the exergy efficiency and unit power cost, confirms that the ANN can be a smart tool to predict the performance of thermodynamic cycles, swiftly, precisely, and robustly.

6. Conclusions

A combined Brayton-organic Rankine flash cycle (ORFC) equipped with a PEM electrolyzer was assessed by the configurations called simple OFRC (SOFRC), dual flash (ODFRC), and improved OFRC (IOFRC). The thermal energy was provided using a biomass-driven fuel. Various working fluids, such as m-xylene, o-xylene, p-xylene, toluene, and ethylbenzene, were examined. The proposed cycle was advantageous in terms of producing several essential energy vectors including hot water, electrical energy, and hydrogen using biomass and waste energy. Energy, exergy, and exergoeconomic analyses were performed. Further, the application of RBF-ANN to predict the results was presented, making the current work distinctive from the existing ones. The main findings of the current study are concisely pointed out as follows.

- The decrement in the exergy destruction by using p-Xylene compared to the case of o-Xylene was respectively 9 %, 12.5 %, and 10 % for SOFRC, ODFRC, and IOFRC, respectively. In terms of higher exergy destruction, the cycles were classified as SOFRC, ODFRC, and IOFRC, respectively.
- IOFRC decreased the exergy destruction by about 10 % compared to SOFRC. The maximum exergy destruction occurred in the SOFRC when o-Xylene was applied.
- The exergy efficiency of the SORFC was lower than that of the other cycles, while IOFRC featured the best exergy efficiency.
- The ODFRC contained a higher unit cost of power produced than the other cycles by a factor of 1.5. The p-Xylene indicated the highest, while o-Xylene showed the lowest unit power cost for all cycles.
- All studied cycles implied a higher investment cost related to the cost of exergy destruction. However, the cycles of a higher share of investment cost ranked as ODFRC, SOFRC, and IOFRC.

Downloaded from https://iranpaper.ir
https://www.tarjomano.com ترجمه تخصصی این مقاله مورد تایید ایران پیپر

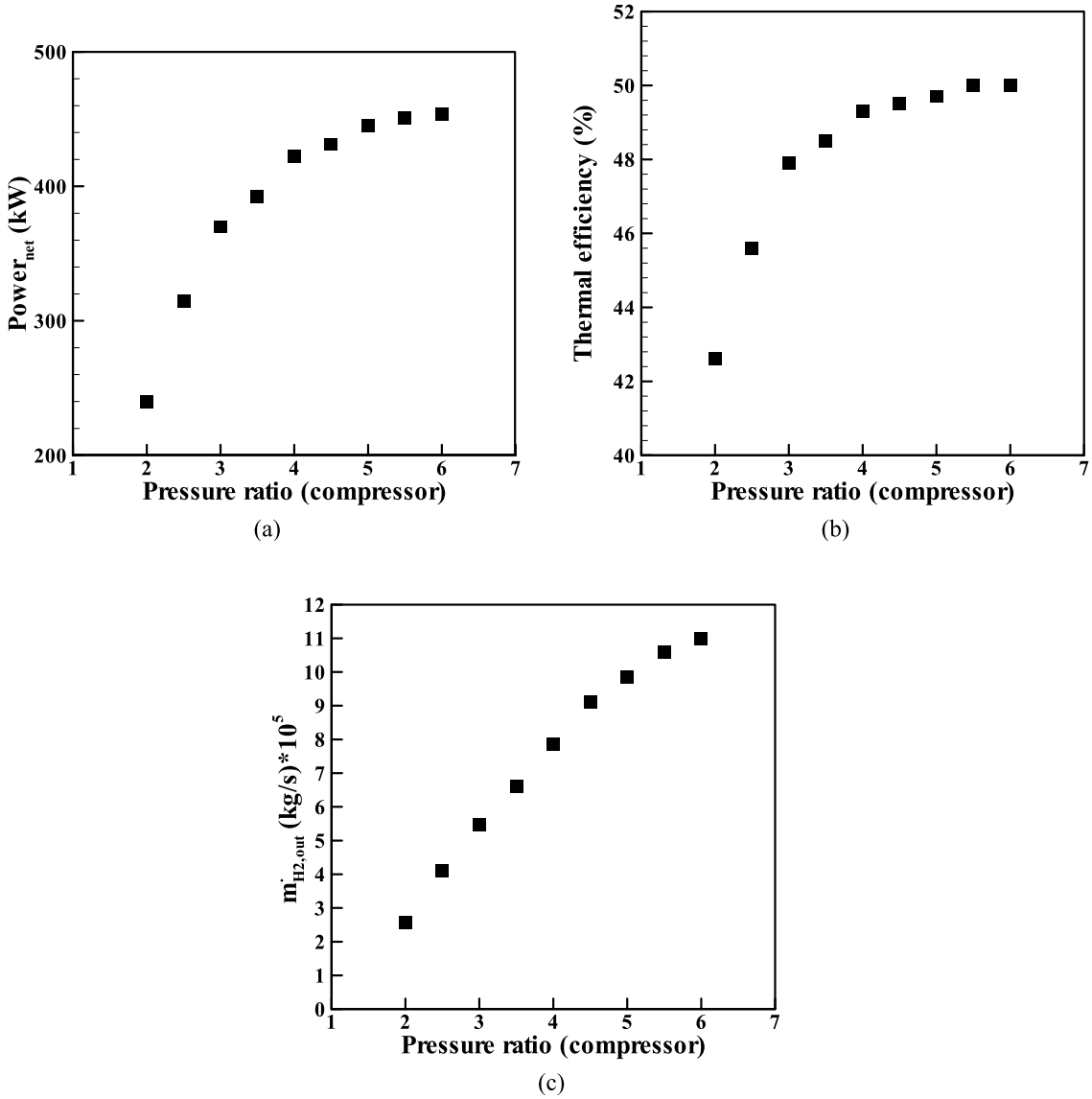

Fig. 10. (a) The net power generation (b) thermal efficiency, and (c) the hydrogen production of the PEM electrolyzer versus pressure ratio of the compressor for IOFRC and p-Xylene under optimum point.

Downloaded from https://iranpaper.ir
https://www.tarjomano.com ترجمه تخصصی این مقاله مورد تایید ایران پیپر

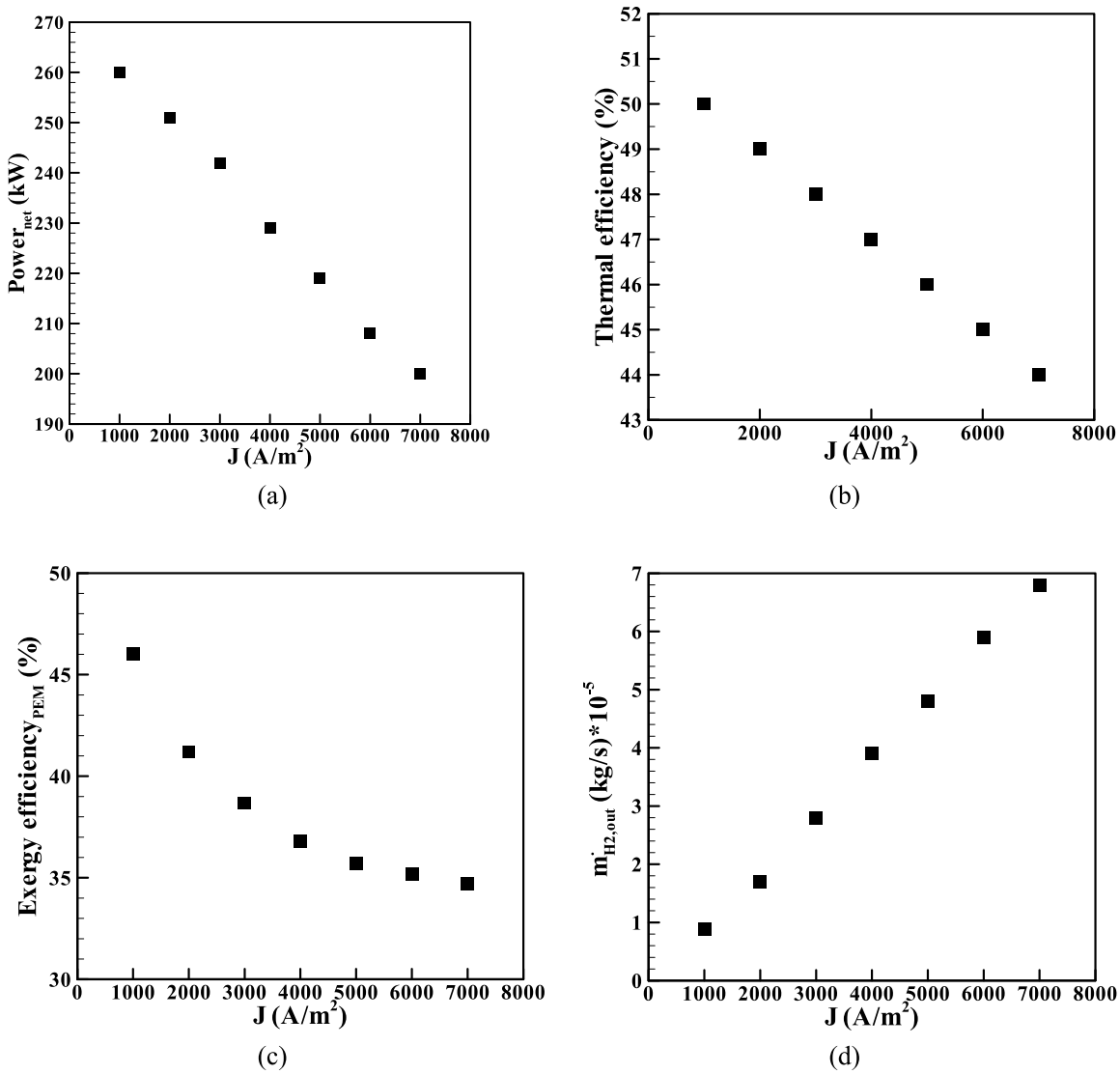

Fig. 11. (a) The net power generation, (b) thermal efficiency, (c) the exergy efficiency of the PEM electrolyzer, and (d) the hydrogen production of the PEM versus the electrolyzer's electrical current for IOFRC and p-Xylene working fluid.

Table 10
A sample of RBF model results.

Type	T_3 (K)	$P_3(kPa)$	Exergy efficiency (%)			Unit power cost ($/GJ)		
			Calculated	Predicted	Error (%)	Calculated	Predicted	Error (%)
IOFRC	450	550	47.11	46.52	1.25	31.3	31.11	0.61
	500	565	48.83	47.30	3.13	30.36	29.62	2.44
	550	580	47.81	47.33	1.00	30.21	30.89	2.25
ODFRC	450	550	46.02	46.93	1.98	43.15	42.88	0.63
	500	565	45.58	46.71	2.48	41.10	40.33	1.87
	550	580	44.13	45.37	2.81	40.46	41.04	1.43
SOFRC	450	550	45.25	46.05	1.77	30.11	30.01	0.33
	500	565	43.83	44.20	0.84	29.85	29.3	1.84
	550	580	41.12	42.28	2.82	28.22	27.79	1.52

- As expected, the cycles were ranked as IOFRC, ODFRC, and SOFRC in terms of having higher thermal efficiency.
- By increasing the electrical current density of the PEM electrolyzer from 1000 to 7000A/m^2, the net power generated subsides by about 23 %, while hydrogen production escalates by about 7 times as more energy is provided for water splitting.
- The precision of RBF-ANN for predictions of the parameters of three proposed cycles was assessed and it was shown that the exergy efficiency and unit power cost could be estimated by the disparity of 2.0 and 1.4 %, respectively. Therefore, the applied AI model can be a precise model to predict the investigated cycles promptly.

Given the analysis of various working fluids for the organic Rankine cycle, particularly the finding that p-Xylene increases exergy efficiency more than other fluids, a practical recommendation would be to consider p-Xylene as a preferable working fluid when designing systems

Downloaded from https://iranpaper.ir
https://www.tarjomano.com ترجمه تخصصی این مقاله مورد تایید ایران پیپر

of this nature. The study suggested that while the application of double flash evaporators improved exergy efficiency, it came at the cost of a significant increase in the unit cost of power generated. Therefore, a practical application of this finding would involve a careful trade-off analysis during the design phase. The application of AI in the thermoecomic design of OFRCs was shown to be so essential. The future work can be concentrated on the generation of some other products, such as those related to making a self-sustainable gasifier in the cycle. Additionally, considering the elements that decrease the exergy destruction, such as a two-stage turbine is also crucial.

CRediT authorship contribution statement

Najmeh Hajialigol: Conceptualization, Project administration, Software, Validation, Visualization. **Abolfazl Fattahi:** Conceptualization, Investigation, Methodology, Software, Visualization. **Nader Karimi:** Data curation, Methodology, Resources, Supervision. **Mostafa Jamali:** Visualization, Writing - review & editing. **Shervin Keighobadi:** Methodology, Validation.

Declaration of competing interest

The authors declare that they have no known competing financial interests or personal relationships that could have appeared to influence the work reported in this paper.

Data availability

Data will be made available on request.

References

[1] Daniarta S, Nemś M, Kolasiński P. A review on thermal energy storage applicable for low- and medium-temperature organic Rankine cycle. Energy 2023;278:127931. https://doi.org/10.1016/J.ENERGY.2023.127931.
[2] Pethurajan V, Sivan S, Joy GC. Issues, comparisons, turbine selections and applications – an overview in organic Rankine cycle. Energy Convers Manag 2018;166:474–88. https://doi.org/10.1016/J.ENCONMAN.2018.04.058.
[3] Kasaeian A, Shamaeizadeh A, Jamjoo B. Combinations of Rankine with ejector refrigeration cycles: recent progresses and outlook. Appl Therm Eng 2022;211:118382. https://doi.org/10.1016/J.APPLTHERMALENG.2022.118382.
[4] V P, Deshmukh D. A comprehensive review of waste heat recovery from a diesel engine using organic rankine cycle. Energy Rep 2021;7:3951–70. https://doi.org/10.1016/J.EGYR.2021.06.081.
[5] Tchanche BF, Pétrissans M, Papadakis G. Heat resources and organic Rankine cycle machines. Renew Sustain Energy Rev 2014;39:1185–99. https://doi.org/10.1016/J.RSER.2014.07.139.
[6] Ho T, Mao SS, Greif R. Increased power production through enhancements to the organic flash cycle (OFC). Energy 2012;45:686–95. https://doi.org/10.1016/J.ENERGY.2012.07.023.
[7] Ho T, Mao SS, Greif R. Comparison of the Organic Flash Cycle (OFC) to other advanced vapor cycles for intermediate and high temperature waste heat reclamation and solar thermal energy. Energy 2012;42:213–23. https://doi.org/10.1016/J.ENERGY.2012.03.067.
[8] Lee HY, Park SH, Kim KH. Comparative analysis of thermodynamic performance and optimization of organic flash cycle (OFC) and organic Rankine cycle (ORC). Appl Therm Eng 2016;100:680–90. https://doi.org/10.1016/J.APPLTHERMALENG.2016.01.158.
[9] Li Z, Lu Y, Huang Y, Qian G, Chen F, Yu X, et al. Comparison study of trilateral rankine cycle, organic flash cycle and basic organic rankine cycle for low grade heat recovery. Energy Proc 2017;142:1441–7. https://doi.org/10.1016/J.EGYPRO.2017.12.532.
[10] Mondal S, De S. Power by waste heat recovery from low temperature industrial flue gas by Organic Flash Cycle (OFC) and transcritical-CO2 power cycle: a comparative study through combined thermodynamic and economic analysis. Energy 2017;121:832–40. https://doi.org/10.1016/J.ENERGY.2016.12.126.
[11] Mondal S, Alam S, De S. Performance assessment of a low grade waste heat driven organic flash cycle (OFC) with ejector. Energy 2018;163:849–62. https://doi.org/10.1016/J.ENERGY.2018.08.160.
[12] Chen LX, Hu P, Sheng CC, Zhang N, Xie MN, Wang FX. Thermodynamic analysis of three ejector based organic flash cycles for low grade waste heat recovery. Energy Convers Manag 2019;185:384–95. https://doi.org/10.1016/J.ENCONMAN.2019.02.016.
[13] Mohammadi Hadelu L, Ahmadi Boyaghchi F. Exergoeconomic and exergoenvironmental analyses and optimization of different ejector based two stage expander-organic flash cycles fuelled by solar energy. Energy Convers Manag 2020;216:112943. https://doi.org/10.1016/J.ENCONMAN.2020.112943.
[14] Mondal S, De S. Ejector based organic flash combined power and refrigeration cycle (EBOFCP&RC) – a scheme for low grade waste heat recovery. Energy 2017;134:638–48. https://doi.org/10.1016/J.ENERGY.2017.06.071.
[15] Baccioli A, Antonelli M, Desideri U. Technical and economic analysis of organic flash regenerative cycles (OFRCs) for low temperature waste heat recovery. Appl Energy 2017;199:69–87. https://doi.org/10.1016/J.APENERGY.2017.04.058.
[16] Mosaffa AH, Zareei A. Proposal and thermoeconomic analysis of geothermal flash binary power plants utilizing different types of organic flash cycle. Geothermics 2018;72:47–63. https://doi.org/10.1016/J.GEOTHERMICS.2017.10.011.
[17] Wu C, Wang S, sen, Li J. Exergoeconomic analysis and optimization of a combined supercritical carbon dioxide recompression Brayton/organic flash cycle for nuclear power plants. Energy Convers Manag 2018;171:936–52. https://doi.org/10.1016/J.ENCONMAN.2018.06.041.
[18] Baccioli A, Antonelli M. Organic Flash Cycles: off-design behavior and control strategies of two different cycle architectures for Waste Heat Recovery applications. Energy Convers Manag 2018;157:176–85. https://doi.org/10.1016/J.ENCONMAN.2017.12.004.
[19] Zheng Z, Cao J. Thermodynamic and feasibility analysis of air conditioning waste heat recovery via power generation cycles. Energy Rep 2020;6:3472–90. https://doi.org/10.1016/J.EGYR.2020.12.005.
[20] Zhao D, Xu W, Zhao R, Deng S, Zhao L. Thermodynamic analysis of the combined organic flash and ejector refrigeration cycle using zeotropic mixtures. Appl Therm Eng 2023;219:119605. https://doi.org/10.1016/J.APPLTHERMALENG.2022.119605.
[21] Zhao D, Deng S, Zhao L, Xu W, Wang W, Nie X, et al. Overview on artificial intelligence in design of organic rankine cycle. Energy AI 2020;1:100011. https://doi.org/10.1016/J.EGYAI.2020.100011.
[22] Liu X, Hu G, Zeng Z. Performance characterization and multi-objective optimization of integrating a biomass-fueled brayton cycle, a kalina cycle, and an organic rankine cycle with a claude hydrogen liquefaction cycle. Energy 2023;263:125535. https://doi.org/10.1016/J.ENERGY.2022.125535.
[23] Wang Q, Macián-Juan R, Li D. Analysis and assessment of a novel organic flash Rankine cycle (OFRC) system for low-temperature heat recovery. Energy Sci Eng 2022;10:3023–43. https://doi.org/10.1002/ESE3.1186.
[24] Wang Q, Wu W, Li D, Wang J, He Z. Thermodynamic analysis and optimization of four organic flash cycle systems for waste heat recovery. Energy Convers Manag 2020;221:113171. https://doi.org/10.1016/J.ENCONMAN.2020.113171.
[25] Wang P, Li Q, Liu C, Wang R, Luo Z, Zou P, et al. Comparative analysis of system performance of thermally integrated pumped thermal energy storage systems based on organic flash cycle and organic Rankine cycle. Energy Convers Manag 2022;273:116416. https://doi.org/10.1016/J.ENCONMAN.2022.116416.
[26] Ai T, Chen H, Zhong F, Jia J, Song Y. Multi-objective optimization of a novel CCHP system with organic flash cycle based on different operating strategies. Energy 2023;276:127577. https://doi.org/10.1016/J.ENERGY.2023.127577.
[27] Hai T, Zoghi M, Abed H, Chauhan BS, Ahmed AN. Exergy-economic study and multi-objective optimization of a geothermal-based combined organic flash cycle and PEMFC for poly-generation purpose. Energy 2023;268:126607. https://doi.org/10.1016/J.ENERGY.2023.126607.
[28] Tang J, Li Q, Wang S, Yu H. Thermo-economic optimization and comparative analysis of different organic flash cycles for the supercritical CO2 recompression Brayton cycle waste heat recovery. Energy 2023;278:128002. https://doi.org/10.1016/J.ENERGY.2023.128002.
[29] Zhou Z, Cao Y, Anqi AE, Zoghi M, Habibi H, Rajhi AA, et al. Converting a geothermal-driven steam flash cycle into a high-performance polygeneration system by waste heat recovery: 3E analysis and Genetic-Fgoalattain optimization. Renew Energy 2022;186:609–27. https://doi.org/10.1016/J.RENENE.2022.01.009.
[30] Yang C, Yi F, Zhang J, Du G, Yin W, Ma Y, et al. Towards high-performance of organic flash cycle through cycle configuration improvement: state-of-art research. Energy 2023;278:127756. https://doi.org/10.1016/J.ENERGY.2023.127756.
[31] Ioroi T, Yasuda K, Siroma Z, Fujiwara N, Miyazaki Y. Thin film electrocatalyst layer for unitized regenerative polymer electrolyte fuel cells. J Power Sources 2002;112:583–7. https://doi.org/10.1016/S0378-7753(02)00466-4.
[32] Habibollahzade A, Mehrabadi ZK, Houshfar E. Exergoeconomic and environmental optimisations of multigeneration biomass-based solid oxide fuel cell systems with reduced CO2 emissions. Int J Energy Res 2021;45:10450–77. https://doi.org/10.1002/ER.6532.
[33] Habibollahzade A, Ahmadi P, Rosen MA. Biomass gasification using various gasification agents: optimum feedstock selection, detailed numerical analyses and tri-objective grey wolf optimization. J Clean Prod 2021;284:124718. https://doi.org/10.1016/J.JCLEPRO.2020.124718.
[34] Ni M, Leung MKH, Leung DYC. Energy and exergy analysis of hydrogen production by a proton exchange membrane (PEM) electrolyzer plant. Energy Convers Manag 2008;49:2748–56. https://doi.org/10.1016/J.ENCONMAN.2008.03.018.
[35] Ahmadi P, Dincer I, Rosen MA. Performance assessment and optimization of a novel integrated multigeneration system for residential buildings. Energy Build 2013;67:568–78. https://doi.org/10.1016/J.ENBUILD.2013.08.046.
[36] Zare V. Exergoeconomic analysis with reliability and availability considerations of a nuclear energy-based combined cycle power plant. Energy 2016;96:187–96. https://doi.org/10.1016/J.ENERGY.2015.12.060.
[37] Cavalcanti EJC, Motta HP. Exergoeconomic analysis of a solar-powered/fuel assisted Rankine cycle for power generation. Energy 2015;88:555–62. https://doi.org/10.1016/J.ENERGY.2015.05.081.

Downloaded from https://iranpaper.ir
https://www.tarjomano.com ترجمه تخصصی این مقاله مورد تایید ایران پیپر

[38] Ahmadi Boyaghchi F, Nazer S. Assessment and optimization of a new sextuple energy system incorporated with concentrated photovoltaic thermal - geothermal using exergy, economic and environmental concepts. J Clean Prod 2017;164: 70–84. https://doi.org/10.1016/J.JCLEPRO.2017.06.194.

[39] Peng H, Long F, Ding C. Feature selection based on mutual information: criteria of max-dependency, max-relevance, and min-redundancy. IEEE Trans Pattern Anal Mach Intell 2005;27:1226–38. https://doi.org/10.1109/TPAMI.2005.159.

[40] Alizadeh R, Najm Mohebbi, Abad J, Fattahi A, Alhajri E, Karimi N. Application of machine learning to investigation of heat and mass transfer over a cylinder surrounded by porous media - the radial basic function network. J Energy Resour Technol Trans ASME 2020;142. https://doi.org/10.1115/1.4047402.

[41] Garcia L, Salvador ML, Arauzo J, Bilbao R. CO2 as a gasifying agent for gas production from pine sawdust at low temperatures using a Ni/Al coprecipitated catalyst. Fuel Process Technol 2001;69:157–74. https://doi.org/10.1016/S0378-3820(00)00138-7.